

1 **Nonlinear hydro-climatic controls on an arid-region lake: Evidence**
2 **from 40 years of remote sensing**

3 Rui Zou^a, Xiaojun Wang^{a,b*}, Jianyun Zhang^{a,b}, Wentai Pang^c, Jianfeng Liu^d

4 ^a The National Key Laboratory of Water Disaster Prevention, Nanjing Hydraulic Research
5 Institute, Nanjing 210029, China

6 ^b Research Center for Climate Change, Ministry of Water Resources, Nanjing 210029, China

7 ^c Academy of Science and Technology of Inner Mongolia, Huhhot 010000, China

8 ^d Water Resources Research Institute of Inner Mongolia, Huhhot 010020, China

9
10
11
12
13
14
15
16
17
18
19
20
21 *** Corresponding Author (Xiaojun Wang) Email: xjwang@nhri.cn.**
22

23 **Abstract:** ~~Accurate~~ Accurate delineation of lake surface area is fundamental for
24 understanding eco-hydrological processes in arid regions, yet long-term lake records
25 are often constrained by cloud contamination, seasonal ice cover, and data gaps. In this
26 study, we develop an optimized lake-area extraction framework that integrates seasonal
27 water-index selection, adaptive threshold segmentation, maximum connected-
28 component analysis, and mutual-information-based image gap filling to construct a
29 continuous monthly lake-area time series for Bahannao Lake from 1984 to 2024. This
30 framework substantially improves the temporal continuity and robustness of long-term
31 monitoring for small lakes in arid environments, and its regional applicability is further
32 validated through comparative analyses with Hongjiannao Lake and Wuliangsuhai
33 Lake. Based on the reconstructed time series, we quantitatively assess the multi-
34 climatic controls on lake-area variability by combining correlation analysis with an
35 XGBoost model. The results reveal pronounced seasonal differences and distinct stage-
36 dependent evolution in lake dynamics, with the dominance alternating between
37 precipitation-driven water input and evaporative demand across different temporal
38 scales. Our findings highlight the nonlinear hydro-climatic responses of arid-region
39 lakes to climate variability and provide both technical support and scientific insight for
40 long-term lake monitoring and water-resource management in dryland
41 regions. ~~measurement of lake surface area is essential for understanding eco-~~
42 ~~hydrological processes in arid regions, yet long-term records are often limited by cloud~~
43 ~~contamination, seasonal ice cover, and data gaps. In this study, we developed an~~
44 ~~optimized extraction framework that integrates seasonal index selection, adaptive~~

45 ~~thresholding, maximum connectivity analysis, and mutual information—based gap~~
46 ~~filling to construct a continuous monthly lake area series for Bahannao Lake from 1984~~
47 ~~to 2024. This method effectively addressed common challenges in remote sensing water~~
48 ~~extraction and provided reliable long-term lake dynamics in a data-scarce desert region.~~
49 ~~Based on the reconstructed time series, we examined the multi-factor drivers of lake~~
50 ~~evolution using an XGBoost model combined with climatic and energy balance~~
51 ~~variables. Results reveal pronounced interannual and seasonal variability: precipitation~~
52 ~~dominates lake expansion in spring and summer, while shortwave radiation is the main~~
53 ~~driver of evaporation in autumn and winter, even under cold conditions. Long-term~~
54 ~~trends indicate a shift in controlling mechanisms—from humidity and precipitation~~
55 ~~decline (1984—1999), to increased radiation and humidity variability (2000—2014),~~
56 ~~and finally to intensified sensible heat flux and potential evapotranspiration (2015—~~
57 ~~2024). Our findings highlight the nonlinear and evolving interactions between hydro-~~
58 ~~climatic factors regulating arid region lakes. The proposed framework provides a robust~~
59 ~~approach for generating long-term lake records, advancing understanding of eco-~~
60 ~~hydrological responses to climate change, and offering scientific support for water~~
61 ~~resources management and adaptation in arid regions.~~

62 **Keywords:** ~~R~~-remote sensing, lake area extraction, XGBoost, arid region, hydro-
63 climatology, ~~climate change~~

66 **1 Introduction**

67 Over the past century, with the intensification of global climate change and the
68 increasing human ability to modify nature, the impact of climate change on lake
69 systems and the surrounding water environment has become more pronounced. The
70 formation and disappearance, expansion and contraction of lakes, as well as changes in
71 water and ecological environments, are the result of interactions among global, regional,
72 and local tectonic activities, climate events, and human activities. Within these systems,
73 a series of complex interactions drive the evolution of lake systems (Ma et al., 2020).

74 Lakes are vital natural resources that are highly sensitive to climate change
75 (Adrian et al., 2009; Schmid et al., 2014). Globally, there are over 100 million lakes,
76 which store 87% of the Earth's liquid surface freshwater. Climate change is one of the
77 most severe threats to global lake ecosystems. As observed in recent decades, lake
78 surface conditions—such as ice cover, surface temperature, evaporation, and water
79 levels—have responded significantly to this threat (Woolway et al., 2020; Tong et al.,
80 2023). Approximately 53% of the world's lakes have experienced a decline in water
81 storage, with a reduction of about 22 billion tons per year. Climate change and human
82 water use have primarily driven the net decrease in water volume in approximately 100
83 large natural lakes worldwide. Lakes in both arid and humid regions are experiencing
84 water loss, with drying trends being more widespread than previously understood.
85 Despite the shrinking of most lakes globally, 24% of lakes and reservoirs have shown
86 a significant increase in water storage. These lakes and reservoirs are mostly located in
87 sparsely populated regions, such as the Tibetan Plateau and the northern Great Plains

88 of North America, as well as areas with newly constructed reservoirs, including the
89 Yangtze River, Mekong River, and Nile River basins (Pickens et al., 2020).

90 China has a vast territory with an extensive network of rivers and lakes. There are
91 2693 lakes with an area greater than 1 km², among which 2557 lakes (95% of the total)
92 have an area between 1 and 100 km². Additionally, there are 10 exceptionally large
93 lakes with an area exceeding 1000 km². The total lake area in China has shown a
94 significant increasing trend, expanding by approximately 7858.53 km² (11.41%) over
95 the past 30 years (Ma et al., 2010; Ma et al., 2011). However, the spatial and temporal
96 imbalance of water resources has intensified, with notable differences in trends across
97 various lake regions. The lake areas in the Tibetan Plateau and Xinjiang regions have
98 increased significantly, contributing 111.55% and 28.41% of the national lake area
99 growth, respectively. In contrast, the lake areas in the Eastern Plain, Inner Mongolia
100 Plateau, Northeast Plain and Mountainous Region, and Yunnan-Guizhou Plateau have
101 declined significantly, with reductions of 24.53%, 9.30%, 6.06%, and 0.54%,
102 respectively. Among these, the Mongolian-Xinjiang Plateau experienced the largest
103 decline in lake numbers, with a loss of 111 lakes. Some lakes in this region have shown
104 signs of shrinkage and salinization (Yang et al., 2010). However, despite increasing
105 attention to global lake changes, small and medium-sized closed-basin lakes in arid and
106 semi-arid regions remain poorly characterized in long-term observations. These lakes
107 are highly sensitive to climate variability but are often underrepresented in existing
108 global or regional datasets, highlighting an urgent need for improved long-term
109 monitoring.

110 Scientists have discovered that the abrupt change timing of river and lake systems
111 varies significantly across different latitudes and altitudes (Råman Vinnå., 2021; Zhou
112 et al., 2021). Mountain and polar lakes tend to experience abrupt changes earlier than
113 temperate and tropical river-lake systems (Jeppesen et al, 2014). Additionally, under
114 varying levels of human impact, the timing of abrupt changes in lakes also differs.
115 Lakes in regions with low human impact generally experience abrupt changes earlier
116 than those in areas with strong human influence (Preston et al., 2016). Analysis of the
117 driving factors of lake abrupt changes indicates that the causes vary. Before the 1950s,
118 climate change was the primary factor controlling abrupt changes in lake ecosystems.
119 However, after the 1950s, both climate change and human disturbances became
120 dominant factors. In temperate and tropical regions with strong human influence, lake
121 changes are mainly driven by nutrient enrichment and pollution. In contrast, lakes
122 located in high-altitude and high-latitude regions, which are less affected by human
123 activities, are more vulnerable to climate change. Furthermore, the interaction of
124 multiple drivers increases the likelihood of abrupt changes in lakes, with climate change
125 being the most frequently interacting factor leading to transformations in river-lake
126 ecosystems (Vincent et al., 2009.). Li et al. (2025) pointed out that seasonality is the
127 dominant driver of lake-surface-extent variations globally

128 For example, Plug et al.(2008) investigated lake area changes in the Tuktoyaktuk
129 Peninsula in northwest Canada. They found that from 1978 to 1992, the total lake area
130 increased, while from 1992 to 2001, the total lake area decreased. Their study identified
131 precipitation as the main factor driving these changes. Similarly, Carroll et al. (2011)

132 studied the lake area changes in high-latitude northern Canada and discovered that lake
133 areas showed a significant decline, exhibiting regional clustering characteristics, with
134 climate factors driving these changes. Labazhuoma et al. (2017) explored the expansion
135 of Tangra Yum Co from 1977 to 2014. Their results indicated that, under the background
136 of climate warming, the combined effects of glacier melt, precipitation increase, and
137 evaporation changes contributed to the lake's expansion. Likewise, Li Meng et al. (2017)
138 examined the changes in the water surface area and water storage of Nam Co from 1976
139 to 2015. Their findings showed that the water surface area and water storage of Nam
140 Co continued to increase, with the fastest growth in water storage occurring between
141 1997 and 2009. The study concluded that the primary factor driving the increase in Nam
142 Co's water volume was glacier melt, followed by increased precipitation and reduced
143 evaporation.

144 However, the precise measurement of lake area remains a major constraint for
145 analyzing lake changes. With advancements in science and technology, remote sensing
146 has provided a unique and effective method for monitoring the spatiotemporal
147 variations in surface water areas on broad geographic scales (Liu et al., 2020).

148 Currently, water extraction methods using optical sensors have been widely
149 applied²⁸⁻³⁰ (McFeeters 1996; Yao et al., 2015; Donchyts et al., 2016). However,
150 existing water body area products often fail to meet ideal spatial or temporal resolution
151 requirements³¹⁻³² (Cooley et al., 2017; Huang et al., 2018). For example, the 2016
152 Global Climate Observing System (GCOS) Implementation Plan recommended a
153 resolution of 20 meters and a daily monitoring frequency (Secretariat, 2009). High-

154 temporal-resolution sensors, such as the Moderate Resolution Imaging
155 Spectroradiometer (MODIS) onboard Terra and Aqua satellites, have been used to
156 assess water body areas at time scales ranging from daily to 16-day intervals (Bergé-
157 Nguyen et al., 2015; Wang et al., 2018). However, many small water bodies (e.g., 10–
158 50 km² or smaller) and irregularly shaped larger water bodies may not be accurately
159 distinguished using coarse-resolution MODIS images (250–500 meters in the visible
160 and near-infrared bands) (Tao et al., 2015). Compared with MODIS, Landsat images
161 (e.g., Landsat 5 Thematic Mapper (TM), Landsat 7 Enhanced Thematic Mapper Plus
162 (ETM+), and Landsat 8 Operational Land Imager (OLI)) offer higher spatial resolution
163 (30 meters) and a temporal resolution of 16 days (or better when combining multiple
164 Landsat sensors). However, due to cloud contamination (Rossow et al., 1999), the
165 actual temporal frequency of water body mapping based on Landsat is often much lower
166 than the nominal resolution and may extend to a year for lakes with persistent ice cover
167 (Yao et al., 2018). The recently launched Sentinel-2A and 2B satellites, equipped with
168 Multispectral Instruments (MSI), provide a resolution of 10 meters in the visible and
169 near-infrared bands, with a revisit period of 5–10 days. However, their observations
170 currently cover only the past few years (since 2015) and are not yet suitable for long-
171 term decadal monitoring.

172 Beyond the trade-offs between spatial and temporal resolution, several other
173 factors challenge high-resolution monitoring of long-term global surface water area
174 changes (Klein et al., 2017). These include the inherent spectral heterogeneity of water,
175 atmospheric influences (clouds and aerosols), topographic shadows, aquatic vegetation,

176 and spectral contamination from ice/snow cover. In such complex conditions,
177 integrating multiple techniques is often necessary to achieve robust water body
178 extraction.

179
180 Recently, Pekel et al. (~~Pekel et al.~~, 2014) utilized a large training dataset, combined
181 with expert systems and visual analysis, to identify the presence or absence of water on
182 a monthly basis for each pixel in archival Landsat images from 1984 to 2015. This
183 product was named the Joint Research Centre (JRC) Global Surface Water dataset
184 (hereinafter referred to as GSW). Despite its significant achievements, GSW is based
185 on cloud-free pixels, meaning that the mapped extent of specific water bodies is only
186 complete when monthly composite images have minimal cloud cover. A follow-up
187 study by Busker et al. (Buske et al., 2019) used a subset of the GSW dataset, selecting
188 images with cloud cover below 5%, to extract the monthly area of 137 lakes/reservoirs.
189 For nearly half of these lakes/reservoirs, the correlation between area and radar
190 altimetry-measured water levels exceeded 0.8. However, the temporal frequency of the
191 resulting area time series was still constrained by the availability of cloud-free images,
192 and due to the current availability of GSW, the time series was interrupted after October
193 2015. One potential method to increase the temporal frequency of lake mapping based
194 on Landsat data is to estimate water surface area from contaminated images (e.g., those
195 affected by clouds or observation gaps). Although these images are of relatively lower
196 quality, the exposed portions of lakes within them may provide useful information for
197 inferring the complete extent. For instance, Zhao and Gao (2018) 41 applied the

198 monthly water mapping data from the GSW dataset to generate area time series for
199 6,817 reservoirs worldwide from 1984 to 2015. Their method involved recovering
200 complete reservoir extents from cloud-contaminated images by segmenting pixels
201 based on the water occurrence probability provided in the GSW dataset. Compared to
202 the results of Busker et al., their generated area time series increased the number of
203 observations by approximately 80%. However, the reliance on the existing GSW dataset
204 restricted their reservoir area records to the 1984–2015 period, and the validation of
205 their recovery method was limited to only nine reservoirs with significant water level
206 variations. These studies demonstrate the feasibility of large-scale lake monitoring, but
207 also highlight persistent limitations related to temporal continuity, cloud dependence,
208 and the applicability of existing products to small lakes. As a result, many existing lake-
209 area studies rely on annual or seasonal snapshots derived from a limited number of
210 cloud-free images, which may obscure important intra-annual variability, abrupt
211 changes, and short-term climate responses, particularly for small lakes with strong
212 seasonal dynamics.

213 To address this limitation, we construct a continuous 40-year monthly lake-area
214 time series for Bahannao Lake by integrating multi-source Landsat imagery and
215 applying a tailored image-processing workflow. This higher-temporal-resolution
216 dataset enables a more detailed assessment of seasonal and interannual lake dynamics.

217
218 Bahannao Lake is a small closed-basin lake located in a semi-arid desert region of
219 northern China. Owing to its remote location and the long-term absence of systematic

220 in situ observations, continuous records of lake area are lacking. Nevertheless, as a
221 water body embedded in a fragile desert ecosystem, variations in lake area are highly
222 sensitive to hydro-climatic changes and play an important role in regional eco-
223 hydrological stability.

224 In recent decades, intensified warming and drying have caused pronounced lake
225 shrinkage, characterized by strong interannual variability and multiple abrupt changes.
226 However, compared with larger or well-monitored lakes, the dynamic behavior and
227 driving mechanisms of Bahannao Lake remain poorly understood due to the lack of
228 long-term, high-temporal-resolution observations. As a typical but underrepresented
229 small lake in arid regions, Bahannao Lake provides an ideal case for testing robust
230 remote-sensing monitoring methods and investigating hydro-climatic controls on
231 dryland lake dynamics~~Bahannao Lake is located in a semi-arid region and has long~~
232 ~~lacked systematic observational data. There are no complete records of its surface area,~~
233 ~~yet its changes are crucial to the stability of the regional ecosystem. With the~~
234 ~~intensification of global climate change, the lake's surface area has significantly shrunk,~~
235 ~~experiencing multiple abrupt shifts and exhibiting a continuous declining trend. The~~
236 ~~driving mechanisms behind these changes are complex and diverse. However, its~~
237 ~~dynamic variation characteristics and driving forces remain insufficiently studied.~~

238 Despite substantial progress in global lake monitoring, significant gaps remain for
239 lakes in arid and semi-arid regions. ~~First,~~ Long-term and continuous lake area records
240 are often interrupted by cloud contamination, seasonal ice cover, and striping artifacts,
241 while the role of hydro-climatic drivers—particularly their nonlinear interactions—

242 ~~remains insufficiently understood~~scarce, as existing products are often interrupted by
243 ~~cloud contamination, seasonal ice cover, and striping artifacts. Second, the role of~~
244 ~~hydro-climatic drivers in regulating lake dynamics remains insufficiently understood,~~
245 ~~particularly regarding nonlinear interactions between precipitation, humidity, radiation,~~
246 ~~and energy fluxes in arid environments. Third, current extraction methods lack~~
247 ~~robustness across different seasons and fail to ensure accuracy in data-scarce regions.~~

248 To address these challenges, this study develops an optimized lake area extraction
249 framework that integrates seasonal index selection, adaptive thresholding, connectivity
250 analysis, and mutual information - based gap filling to construct a continuous monthly
251 ~~lake-area record for Bahannao Lake from 1984 to 2024~~record of Bahannao Lake from
252 1984 to 2024. By coupling ~~the~~ this reconstructed time series with multi-factor analysis
253 using the XGBoost model, we quantify the relative importance and nonlinear effects of
254 key hydro-climatic drivers on lake dynamics. This framework not only improves the
255 reliability of long-term lake monitoring under complex conditions, but also provides
256 new insights into seasonal and interannual climate controls on small lakes in arid and
257 semi-arid regions.~~reveal the temporal shifts and nonlinear controls of hydro-climatic~~
258 ~~drivers on lake dynamics. This framework not only improves the reliability of long-~~
259 ~~term lake monitoring under complex conditions but also advances understanding of~~
260 ~~eco-hydrological responses to climate change and provides implications for water~~
261 ~~resource management in arid regions.~~

262 **2 Data and Methods**

263 **2.1 Dataset Selection**Study area and data

264 Closed-basin lakes of various sizes are widely distributed across the Ordos Plateau,
265 formed since the late Quaternary through combined aeolian and fluvial erosion
266 processes. Bahannao Lake is the terminal basin of a chain of seven bead-like erosional
267 lake depressions that developed along an ancient river valley. Bahannao Lake (109°
268 16' E, 39° 19' N) is located in the central Ordos Plateau at an elevation of 1278 m,
269 with a lake-basin area of 26.50 km². The basin is underlain by a continuous and intact
270 Lower Cretaceous sandstone formation, which provides a closed geomorphic setting
271 primarily recharged by atmospheric precipitation. The sandstone contains abundant
272 sodium- and calcium-rich carbonates, serving as the major source of dissolved salts in
273 Bahannao Lake. Administratively, the study area belongs to Wushen Banner of the
274 Ordos region in Inner Mongolia (Figure 1).

275 The zonal vegetation is dominated by arid to semi-arid desert steppe. The region
276 is controlled for most of the year by the northwesterly monsoon, resulting in a cold and
277 dry climate, while the southeasterly monsoon occasionally influences the area and plays
278 a decisive role in seasonal precipitation. The mean annual temperature ranges from 6 to
279 9 °C, and the mean annual precipitation is only 200 – 300 mm, concentrated mainly
280 from June to September with short-duration high-intensity rainfall events. In contrast,
281 the annual potential evaporation reaches 2500 – 3000 mm, approximately ten times the
282 precipitation amount, and the regional aridity index ranges from 3.5 to 4.0.

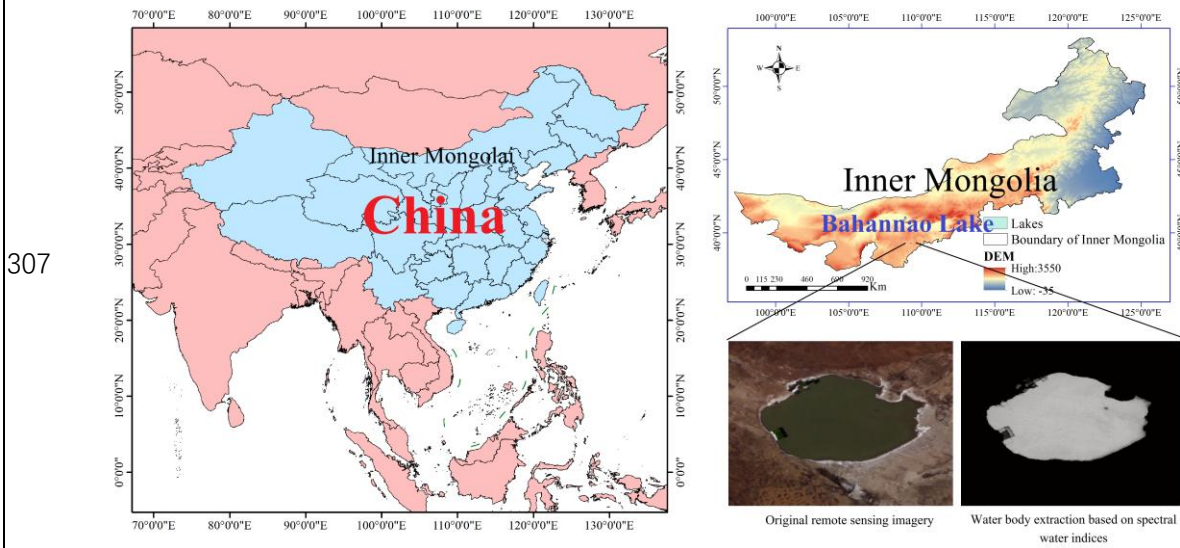
283 Because of the extremely fragile water balance and rapid hydrological response to

284 climatic anomalies, Bahannao Lake and other nearby lakes are widely recognized as
285 important natural indicators of climate variability, drought intensification, and land –
286 atmosphere interactions in the arid and semi-arid regions of northern China.

287 This study utilizes remote sensing imagery from the Landsat 5 TM, Landsat 7 TM,
288 and Landsat 8 OLI sensors, specifically using atmospherically corrected reflectance
289 data (Tier 1 TOA Reflectance). Tier 1 data is selected due to its highest quality, making
290 it suitable for time-series analysis and studies on global surface water extent and
291 dynamics. The Landsat 5 TM imagery covers the period from 1984 to 2011, while
292 Landsat 8 imagery spans from 2013 to 2023. Since imagery for 2012 is missing in both
293 datasets, Landsat 7 TM is used as a supplement. However, Landsat 7 TM imagery
294 exhibits significant striping artifacts, which were avoided as much as possible during
295 data selection.

296 For hydro-climatic elements~~meteorological data~~, this study employs the fifth-
297 generation atmospheric reanalysis dataset from ECMWF (European Centre for
298 Medium-Range Weather Forecasts), covering global climate data from January 1950 to
299 the present. The dataset has a temporal resolution of daily and a spatial resolution of
300 $0.1^{\circ} \times 0.1^{\circ}$. The hydro-climatic variables used in this study include precipitation (P, mm),
301 air temperature at 2 m (T, ° C), 2 m dew point temperature (Td, ° C), relative
302 humidity (RH, %), potential evapotranspiration (PET, mm), net shortwave radiation at
303 the surface (msnswrf, $W m^{-2}$), net longwave radiation at the surface (msnlwrf, $W m^{-2}$),
304 surface latent heat flux (mslhf, $W m^{-2}$), and surface sensible heat flux (msshf, $W m^{-2}$).
305 These variables jointly characterize atmospheric moisture conditions, energy balance,

306 and evaporative demand in the study region.



308 Figure 1 Overview map of the study area

309

310 **2.2 Methods**

311 (1)2.2.1 Optimized Lake-lake Area-area Extraction-extraction Methodmethod

312 Although water-index-based lake extraction from Landsat imagery is well
313 established, long-term monthly monitoring of small lakes in arid regions poses specific
314 challenges, including frequent cloud contamination, striping artifacts in ETM+ data,
315 and strong intra-annual variability. To address these issues, we developed an optimized
316 processing workflow tailored to long-term monthly lake monitoring.

317 This study employs 30-meter full-atmosphere imagery from the Landsat 5
318 Thematic Mapper (TM), Landsat 7 Enhanced Thematic Mapper Plus (ETM+), and
319 Landsat 8 Operational Land Imager (OLI) satellites to derive monthly lake area
320 estimates for the study region from January 1984 to December 2024.

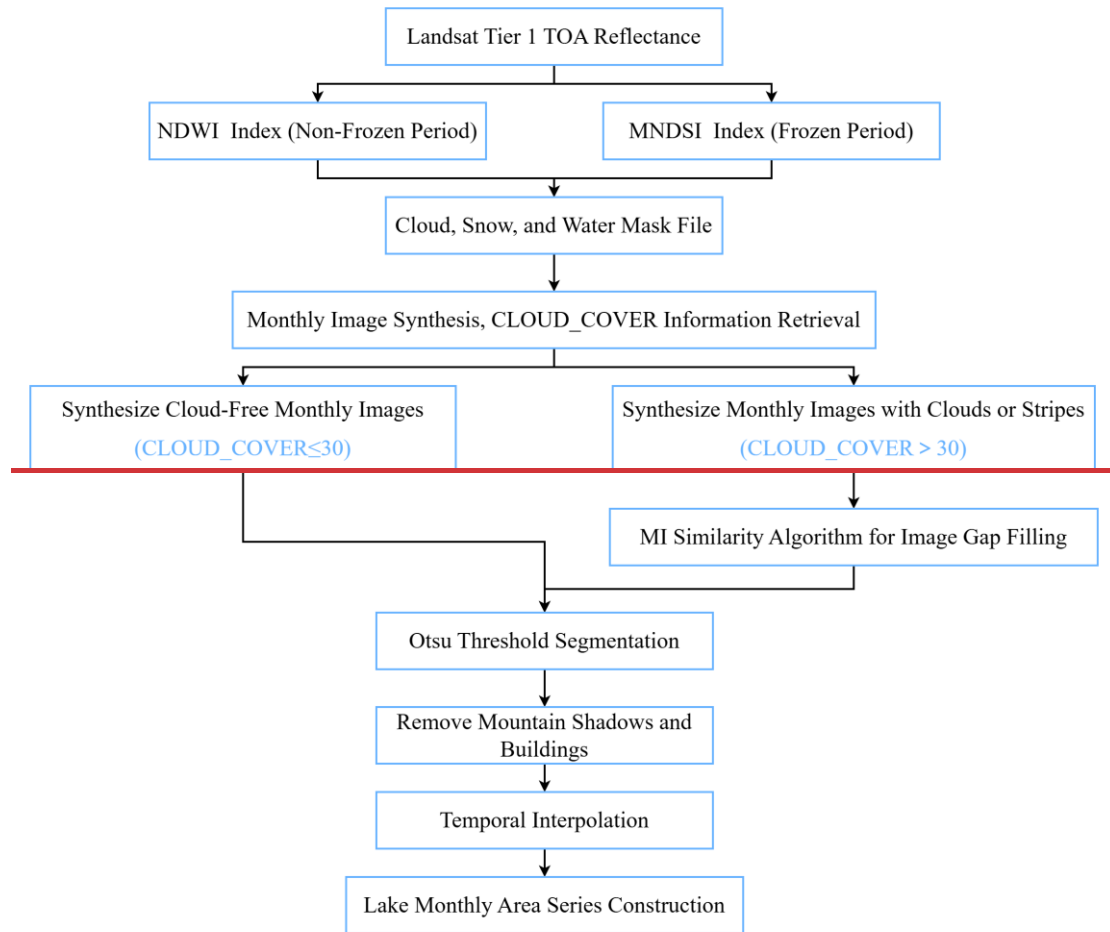
321 Different lake remote sensing indices were selected for non-freezing and freezing

322 periods, respectively. For non-freezing periods, remote sensing indices were processed
323 to remove cloud and snow interference. Images were filtered based on cloud cover
324 percentage (C), and monthly composite images were generated. The Otsu thresholding
325 method was then applied to automatically determine segmentation thresholds. To
326 distinguish between lakes and mountainous areas, a digital elevation model (DEM) was
327 used, setting the slope (θ) and aspect (ϕ) thresholds to 0.

328 Considering that most lakes exhibit connectivity, this study adopts the maximum
329 connected component analysis algorithm from the OpenCV computer vision library to
330 delineate lake boundaries. Images were categorized based on cloud cover information
331 ('CLOUD_COVER'): those with cloud cover $\leq 30\%$ were classified as cloud-free
332 images, while the remaining images were considered cloudy. For cloudy images, the
333 MI (Mutual Information) algorithm was used to match them with the most similar
334 cloud-free images. The most similar image was then merged with the original cloudy
335 image to generate a filled version.

336 For images with striping artifacts, the same filling method was applied as for
337 cloudy images. Clear lake boundaries from historical cloud-free images were used, and
338 the MI algorithm was employed to find the most similar historical cloud-free images
339 for filling missing water pixels in striped areas, ultimately obtaining the final lake water
340 extent. The specific process is shown in Figure 12.

341



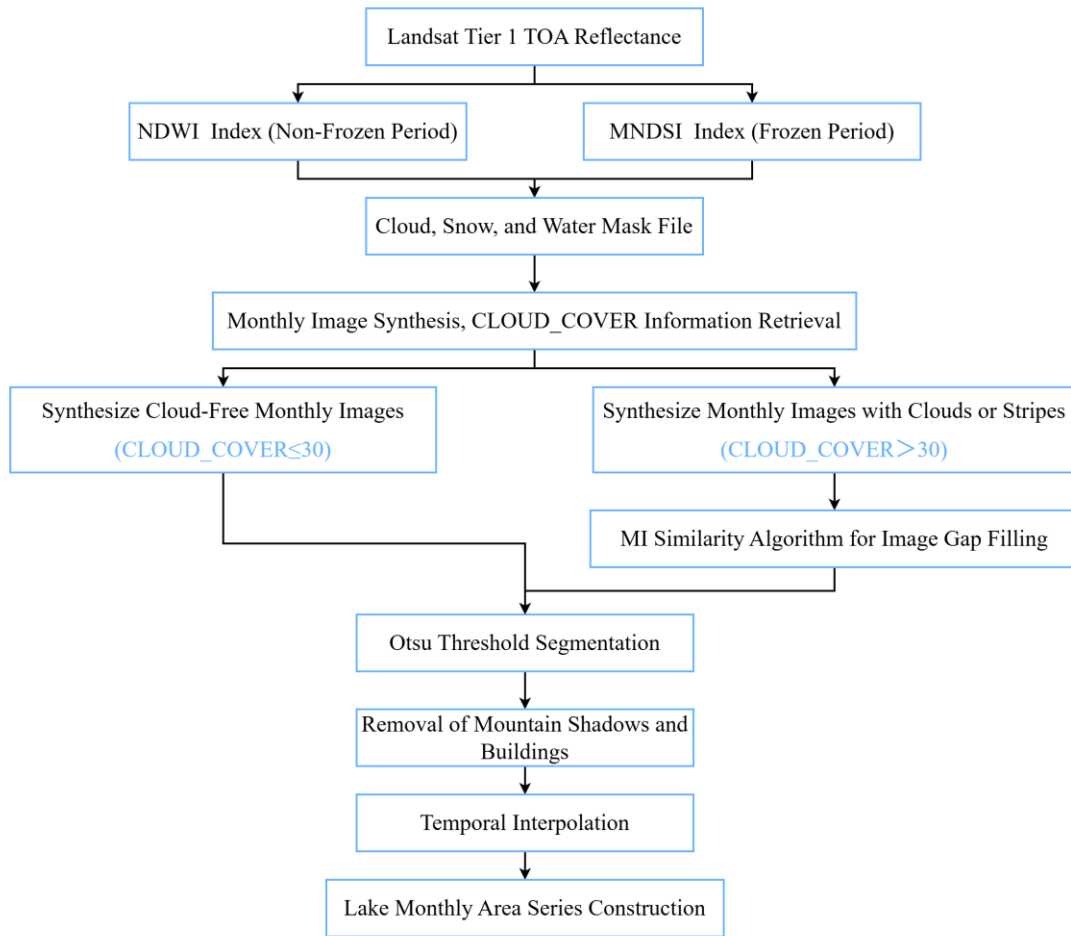


Figure 12. Flowchart of Lake-lake Area-area Extraction-extraction Processprocess-

2.2.2 Aridity index (AI)

The aridity index (AI) was used to quantify regional drought conditions. AI is defined as the ratio of precipitation (P) to potential evapotranspiration (PET), expressed as:

$$AI = \frac{P}{PET} \quad (1)$$

where P represents precipitation and PET denotes potential evapotranspiration. AI reflects the balance between atmospheric water supply and evaporative demand.

In this study, PET was calculated using the FAO Penman - Monteith method, which is widely recognized as a physically based and robust approach for estimating

353 atmospheric evaporative demand. PET was computed as:

$$354 \quad \text{PET} = \frac{0.408\Delta(R_n - G) + \gamma \frac{900}{T + 273} u_2 (e_s - e_a)}{\Delta + \gamma(1 + 0.34u_2)} \quad (2)$$

355 Where R_n is the net radiation at the surface ($\text{MJ m}^{-2} \text{ day}^{-1}$), G is the soil heat flux
356 ($\text{MJ m}^{-2} \text{ day}^{-1}$), T is the mean air temperature at 2 m height ($^{\circ}\text{C}$), u_2 is the wind speed
357 at 2 m height (m/s), e_s is the saturation vapor pressure (kPa), e_a is the actual vapor
358 pressure (kPa), Δ is the slope of the saturation vapor pressure - temperature curve
359 ($\text{kPa } ^{\circ}\text{C}^{-1}$), and γ is the psychrometric constant ($\text{kPa } ^{\circ}\text{C}^{-1}$).

360 All meteorological variables required for PET estimation were obtained from the
361 ERA5 reanalysis dataset and spatially averaged over the study area to ensure
362 consistency with basin-scale analysis.

363 Based on AI values, climatic conditions were classified following the United
364 Nations Environment Programme (UNEP) scheme: $\text{AI} < 0.05$ indicates hyper-arid
365 conditions, $0.05 \leq \text{AI} < 0.20$ represents arid conditions, $0.20 \leq \text{AI} < 0.50$
366 corresponds to semi-arid conditions, $0.50 \leq \text{AI} < 0.65$ indicates dry sub-humid
367 conditions, and $\text{AI} \geq 0.65$ represents humid conditions. This classification allows a
368 quantitative interpretation of regional aridity and facilitates comparison with previous
369 studies in arid and semi-arid regions.

370 2.2.3(2)-XGBoost Model

371 In this study, the XGBoost model is employed primarily as an interpretative tool.
372 The objective is to quantify the relative importance of different hydro-climatic factors
373 and to explore potential nonlinear relationships between lake-area variability and

374 climatic drivers. Given the limited sample size, strong interannual variability, and high
375 nonlinearity characteristic of arid-region lake systems, model performance metrics (e.g.,
376 R²) are used as auxiliary indicators, while greater emphasis is placed on feature-
377 importance rankings for mechanism interpretation.

378 Compared with linear correlation analysis, the XGBoost results highlight the
379 importance of nonlinear and season-dependent controls, particularly during transitional
380 seasons when linear correlations are weak. This demonstrates the added value of
381 XGBoost in revealing climatic influences that cannot be fully captured by linear
382 statistical methods alone.

383 The objective function of the XGBoost model is:

$$384 \quad L(\theta) = \sum_{i=1}^n l(y_i, f(x_i)) + \sum_{k=1}^n \Omega(f_k) \quad (3)$$

385 —
386 Where $L(\theta)$ represents the objective function, which measures the model's
387 performance in prediction and consists of two parts: $l(y_i, f(x_i))$ is the loss function,
388 indicating the difference between the true value y_i and the predicted value $f(x_i)$,
389 while $\Omega(f_k)$ is the regularization term used to control the model complexity.

390 The input factors $x_i = \{x_1, x_2, \dots, x_n\}$ include ~~various environmental variables such~~
391 ~~as temperature, precipitation, humidity, and radiation.~~ precipitation (P), air temperature
392 (T), relative humidity (RH), and potential evapotranspiration (PET), which represent
393 the primary components of the lake water balance in arid and semi-arid regions. These
394 variables directly or indirectly regulate lake-area changes through their influence on
395 water input and evaporative loss. Energy-related variables (e.g., radiation and heat

396 fluxes) are included as background indicators of atmospheric conditions and are not
397 interpreted as direct driving forces of lake-area change.

$$398 \quad FI(x_j) = \frac{1}{T} \sum_{t=1}^T I(t, x_j) \quad (4)$$

399
400 Here, $FI(x_j)$ represents the feature importance of factor x_j , while $I(t, x_j)$
401 denotes the contribution of factor x_j when used as a splitting point in tree t , with T
402 being the total number of trees. The generated feature importance ranking chart
403 illustrates the contribution of various input factors (such as temperature, precipitation,
404 and humidity) to lake area changes. This ranking chart provides an intuitive way to
405 identify the most influential factors.

406
407 To improve model performance, hyperparameters can be optimized using Grid
408 Search or Random Search. Common hyperparameters include Learning rate, Max depth
409 of trees and Number of trees. Adjusting these parameters affects the model's fitting
410 ability and generalization performance.

411 Data Splitting: Divide the dataset into a training set and a test set (e.g., 80% for
412 training, 20% for testing).

413 Train the XGBoost model on the training set. XGBoost uses the Gradient Boosting
414 Algorithm, which iteratively improves the model by building multiple weak learners to
415 reduce prediction errors. Each iteration refines the model by fitting the residuals (i.e.,
416 prediction errors).—

417 Model Validation: Evaluate model performance using metrics such as Mean

438 with linear correlation analysis to provide a more robust understanding of hydro-
439 climatic controls.

441 **3. Lake Area-area Time-time Series-series Constructionconstruction**

442 **3.1 Remote Sensing-sensing Interpretation-interpretation and Monthly-monthly**

443 **Lake-lake Image-image Synthesisynthesis**

444 **(1) 3.1.1 Selection of water indices and image preprocessing** 445 **Selection of Remote Sensing Indices**

446 The study area is located in a high-altitude region, where lake surfaces freeze
447 between November and March. Since the NDWI index is less effective for frozen lakes,
448 different indices are used for different seasons. During the non-freezing period (May–
449 November), the NDWI index is applied for conventional water body extraction. During
450 the freezing period (December–April), the Modified Normalized Difference Snow
451 Index (MNDSI) is used to evaluate water surface area.

452 The NDWI index utilizes the strong absorption of water bodies in the near-infrared
453 band and their high reflectance in the green band to enhance the distinction between
454 water and other land cover types. However, this index may misidentify bright white
455 buildings, clouds, snow, and mountain shadows as water bodies. Therefore, additional
456 data quality bands and methods are integrated to remove these interferences and
457 improve the accuracy of water body extraction.

$$458 \quad \underline{NDWI = \frac{(Green - NIR)}{(Green + NIR)}} \quad (8)$$

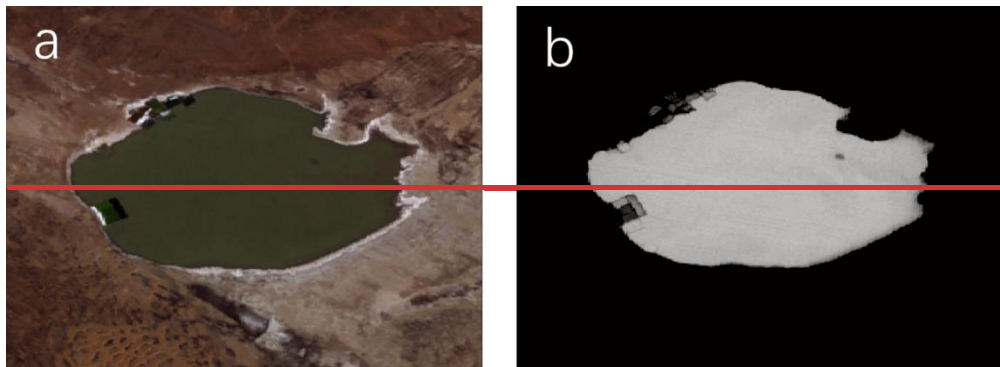
459

460

Where: Green band typically refers to the green portion of the visible spectrum, generally ranging from 500–570 nm. NIR band refers to the near-infrared spectrum, generally ranging from 800–900 nm.

461

462



463

464

~~Figure 2 Original lake image during the non-freezing period (a) and NDWI identified image (b). Source: Landsat imagery courtesy of the U.S. Geological Survey (USGS), processed and interpreted by the authors.~~

465

466

467

The Modified Normalized Difference Snow Index (MNDSI) is an index calculated using the reflectance of the near-infrared (NIR) and short-wave infrared (SWIR) bands.

468

469

It is an effective method for distinguishing ice surfaces from water bodies. This index

470

is particularly suitable for regions with frozen water surfaces, such as lakes and rivers,

471

where seasonal changes are significant. Ice surfaces and water bodies have different

472

reflectance characteristics in various bands. Ice has higher reflectance in the SWIR band,

473

while water has lower reflectance. By calculating the difference between the NIR and

474

SWIR bands, MNDSI can effectively distinguish between ice surfaces and water bodies,

475

thus improving the accuracy of ice extraction. By combining these two bands, MNDSI

476

highlights the differences between water bodies and ice surfaces, making it easier to

477

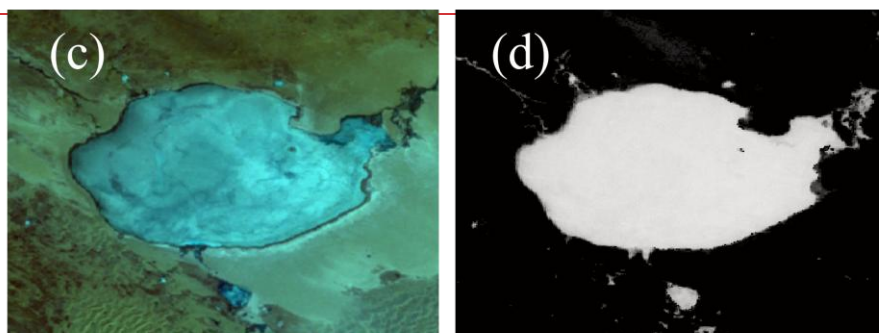
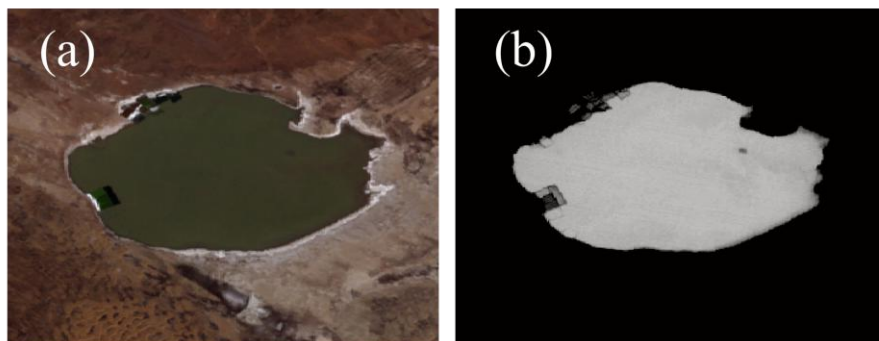
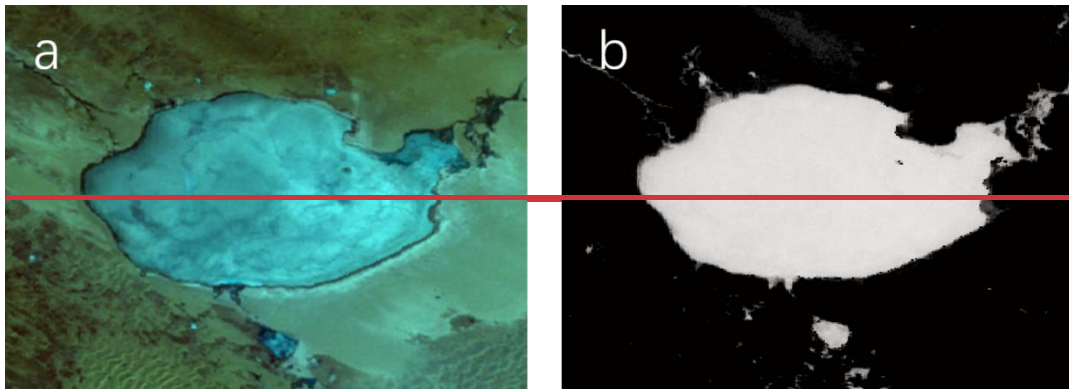
differentiate between them. Similar to NDWI, MNDSI enhances the contrast between

478 ice and water by utilizing reflectance values from different bands.

479 MNDSI (Modified Normalized Difference Snow Index) is calculated by
480 combining the reflectance of the near-infrared (NIR) and short-wave infrared (SWIR)
481 bands. The typical formula for MNDSI is as follows:

$$482 \quad \text{MNDSI} = \frac{\text{NIR} - \text{SWIR}}{\text{NIR} + \text{SWIR}} \quad (9)$$

484 Where NIR is the reflectance in the near-infrared band (typically 800–900 nm),
485 SWIR is the reflectance in the short-wave infrared band (typically 1500–1700 nm).



488 Figure 3 Lake extraction from Landsat imagery during non-freezing and freezing
489 periods. Figure 2 (a) Original Landsat image during the non-freezing period; (b) Lake area identified
490 using NDWI; (c) Original Landsat image during the freezing period; (d) Lake area identified using
491 MNDSI Original lake image during the non-freezing period (a) and NDWI-identified image (b).
492 Source: Landsat imagery courtesy of the U.S. Geological Survey (USGS), processed and interpreted
493 by the authors.

494 ~~Figure 3 Original image of the lake during the freezing period (a) and MNDSI~~
495 ~~recognition image (b). Source: Landsat imagery courtesy of the U.S. Geological Survey~~
496 ~~(USGS), processed and interpreted by the authors.~~

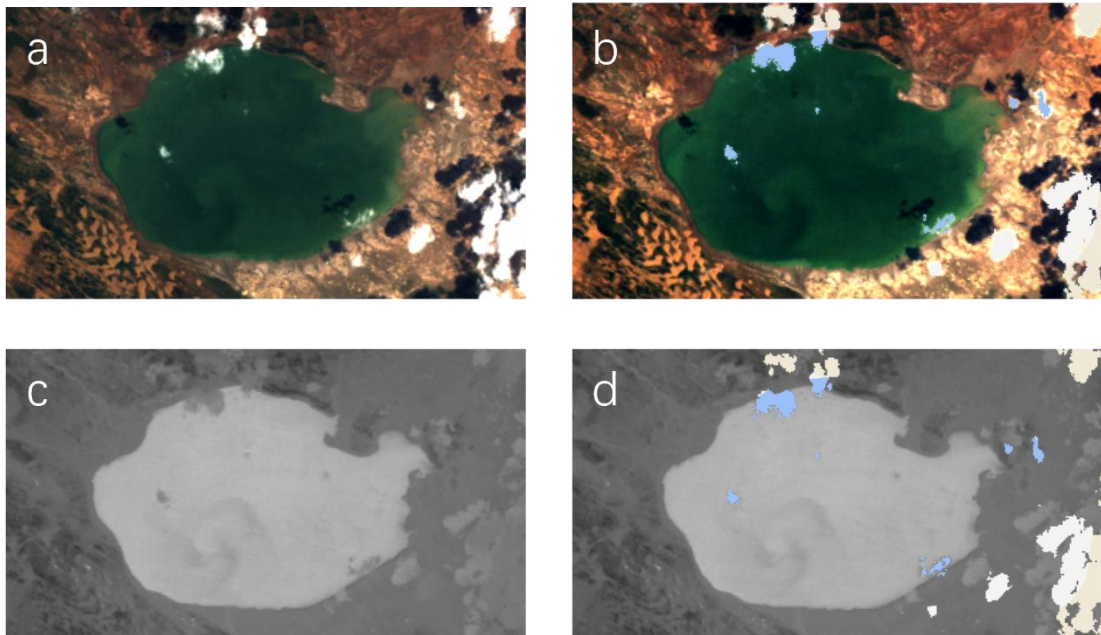
497 ~~(3) Cloud and Snow Interference Removal~~

498 The cloud and snow interference removal is only applied to the NDWI of the non-
499 freezing period from May to November. The Landsat series satellites provide their own
500 pixel-scale data quality band (QA_PIXEL), which can be used to eliminate noise pixels
501 in the image.

502 The QA_PIXEL band in the Landsat dataset provides information on various
503 quality types, where different bits (Bit) correspond to different types of quality
504 information. For example, Bit 3 corresponds to clouds, Bit 5 corresponds to snow, and
505 Bit 7 corresponds to water bodies. Within the same bit, values of 0 and 1 represent
506 different data qualities. For example, a 0 in Bit 7 indicates that the pixel has poor water
507 body information, being land or covered by clouds, while a 1 indicates that the pixel
508 represents water.

509 Using this pixel quality information, we selected Bit 3 (cloud), Bit 5 (snow), and

510 Bit 7 (water body). By performing bitwise AND and OR operations, we generated a
511 water body mask file with good data quality after cloud and snow removal. This mask
512 file is then overlaid with the actual image to remove pixels affected by cloud or snow
513 interference. The effect of cloud and snow removal is shown in the image below:



514

515 Figure 4. Illustration of cloud and snow removal and its effect on NDWI-based water extraction.
516 (a) True-color Landsat image before cloud and snow removal. (b) True-color image after cloud and
517 snow masking, where contaminated pixels are excluded. (c) NDWI image derived from the original
518 true-color image, shown in grayscale, with brighter values indicating higher likelihood of water
519 presence. (d) NDWI image after cloud and snow removal; blue areas indicate pixels affected by
520 cloud or snow that were excluded from water-body extraction. Source: Landsat imagery courtesy of
521 the U.S. Geological Survey (USGS), processed and interpreted by the authors.~~Figure 4: True-color~~
522 ~~original image (a), true-color image after cloud and snow removal (b), NDWI water body index~~
523 ~~calculation result of the true-color original image (c), NDWI water body index calculation result of~~
524 ~~the true-color image after cloud and snow removal (d). Source: Landsat imagery courtesy of the U.S.~~

525 ~~Geological Survey (USGS), processed and interpreted by the authors.~~

526 ~~(4) Monthly Image Download~~

527 The NDWI, MNDSI index calculation, and cloud/snow interference removal are
528 performed directly on the GEE platform, followed by monthly composite image
529 downloads. Based on the cloud cover information ('CLOUD_COVER'), which
530 represents the cloud amount (range from 0 to 100, with larger values indicating more
531 cloud coverage), the data is classified into three levels: 0-30, 30-60, and 60-100. If data
532 is available in Level 1, Level 2 is not executed, and if Level 2 contains data, Level 3 is
533 processed. All images from each year and month within the cloud cover level are
534 selected, and the median pixel value is calculated to generate the composite monthly
535 NDWI (for 5-11 months) and MNDSI (for December to the following April) grayscale
536 images.

537 Data is filtered based on the cloud cover proportion C , where $C \in [0,100]$.

538 Composite image=Med($S(C)$), where $C=CLOUD_{COVER}$

$$539 \quad S(C) = \begin{cases} I(C) & \text{if } 0 \leq C \leq 30 \\ I(C) & \text{else if } 30 < C < 60 \\ I(C) & \text{else } 60 < C \leq 100 \end{cases} \quad (10)$$

541 Where $I(C)$ is a set of image data filtered by cloud cover.

542 3.1.2 Threshold-based water segmentation and noise removal

543 Lake water pixels were first identified using threshold-based segmentation. To
544 reduce false positives caused by mountain shadows and built-up areas, topographic and
545 ancillary data were applied to remove non-water pixels.

546 (5.1) Threshold Segmentation

547 This step applies the Otsu threshold algorithm to the downloaded NDWI and
548 MNDSI monthly composite grayscale images, automatically generating a segmentation
549 threshold. Pixels below the threshold are classified as water, and those above the
550 threshold are classified as other areas.

551 The core of the Otsu thresholding method is to divide the image into two classes
552 (foreground and background) by maximizing the between-class variance, thereby
553 achieving the optimal threshold segmentation. Specifically, it involves iterating through
554 all possible thresholds, and the optimal threshold is determined when the between-class
555 variance is maximized while the variance within both the foreground and background
556 is minimized. Compared to other methods, this algorithm maximizes the inclusion of
557 the target feature while excluding other interfering factors.

558 The Otsu thresholding method is used to automatically generate the segmentation
559 threshold, dividing the image into water and other regions:

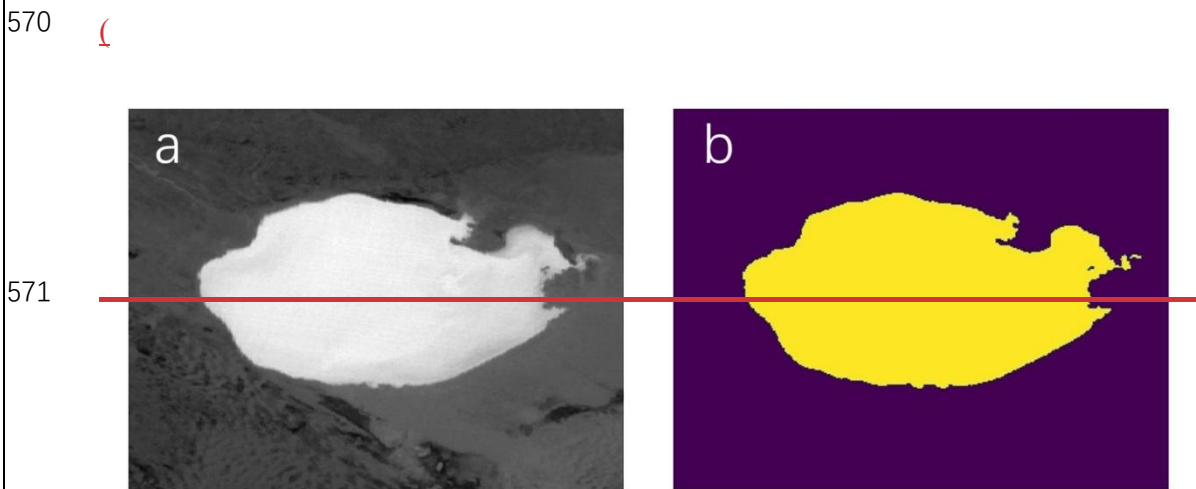
$$T = \arg \max \max(\sigma_B^2(\tau)) \quad (11)$$

561
562 Where, $\sigma_B^2(\tau)$ is the between-class variance, defined as:

$$\sigma_B^2(\tau) = \omega_1(\tau)\omega_2(\tau)(\mu_1(\tau) - \mu_2(\tau))^2 \quad (12)$$

563
564
565 Where $\omega_1(\tau)$ and $\omega_2(\tau)$ are the weights of the foreground and background at
566 the threshold τ , and $\mu_1(\tau)$ and $\mu_2(\tau)$ are the mean gray values of the foreground and
567 background, respectively.

568 The portion smaller than the threshold T is classified as water, symbolized as water
569 pixels, while the portion greater than the threshold is classified as other categories.



572 ~~Figure 5 NDWI water index recognition result (a), and the effect of Otsu threshold~~
573 ~~method automatically separating water (yellow area) and background (purple area)~~
574 ~~based on NDWI recognition result (b). Source: Landsat imagery courtesy of the U.S.~~
575 ~~Geological Survey (USGS), processed and interpreted by the authors.~~

576 ~~(62) Mountain Shadow shadow and buildings Removalremoval~~

577 Since the lake surface typically exhibits a flat state without significant slope and
578 aspect features, digital elevation models (DEM) can be used to distinguish lakes from
579 mountainous regions by utilizing slope and aspect information. By setting threshold
580 values of 0 for slope and aspect, the distinction between lakes and mountainous areas
581 can be made. However, the current frequency of elevation data updates does not align
582 with real-time imagery, leading to an inability to accurately reflect seasonal changes in
583 lake water levels within the elevation data. This limitation affects the precision of water
584 body area extraction using the data. Given that most lakes are interconnected, this study
585 employs the maximum connected component analysis algorithm from the Open-CV

586 vision field to define the boundaries of lakes and extract their areas.

587 By setting the thresholds for slope θ and aspect ϕ to 0 in the digital elevation model
588 (DEM), lakes are distinguished from mountainous areas:

$$589 \quad \theta(x, y) = 0, \quad \phi(x, y) = 0 \quad (13)$$

590
591 Where $\theta(x, y)$ and $\phi(x, y)$ represent the slope and aspect values at a given
592 point (x, y) , respectively. By setting $\theta(x, y) = 0$ and $\phi(x, y) = 0$ as threshold
593 conditions for the lake area, the lake region is defined as the area where both the slope
594 and aspect are equal to 0.

$$595 \quad L = \max_i \left(\sum_{(x,y) \in C_i} I(x, y) \right) \quad (14)$$

596
597 Where L represents the total number of pixels in the largest lake area, C_i
598 represents the i -th connected component in the image, the function \sum denotes the
599 summation of pixel points, and \max_i indicates the selection of the largest connected
600 component as the lake area.

601 602 ~~(7) Buildings Removal~~

603 The construction of the building index currently mainly relies on the fact that the
604 surface temperature of buildings is usually higher than that of surrounding land cover,
605 and the mid-infrared band can effectively reflect surface temperature differences.

606 However, in previous land cover classification studies, the extraction results using this
 607 algorithm were not ideal. Considering that most buildings in the study area are not
 608 distributed along lakes, the maximum connected component algorithm can effectively
 609 exclude parts where buildings are misidentified as water bodies.

610 Based on the NDWI (Normalized Difference Water Index), a threshold T is used
 611 to binarize the image, separating water bodies from non-water bodies.

$$612 \quad I(x, y) = \begin{cases} 1, & \text{if } NDVI(x, y) > T \\ 0, & \text{if } NDVI(x, y) \leq T \end{cases} \quad (15)$$

613
 614 Connected Component Calculation: In the binarized image, the Connected
 615 Components Labeling (CCL) algorithm is used to identify all connected regions. A
 616 connected component is determined by scanning the neighboring pixels in the image
 617 (up, down, left, right, or diagonally). The formula is expressed as:

$$618 \quad C_i = \sum_{(x,y) \in R} I(x, y) \quad (16)$$

619
 620 Where R represents the connected regions in the image, and C_i denotes the
 621 connected components.

622 To eliminate interference from buildings, a threshold condition τ is set, retaining
 623 only connected components with an area greater than τ . Since buildings typically have
 624 smaller areas, while lakes exhibit larger connected components, the lake regions can be
 625 filtered using the following condition:

626
$$C_i > \tau \tag{17}$$

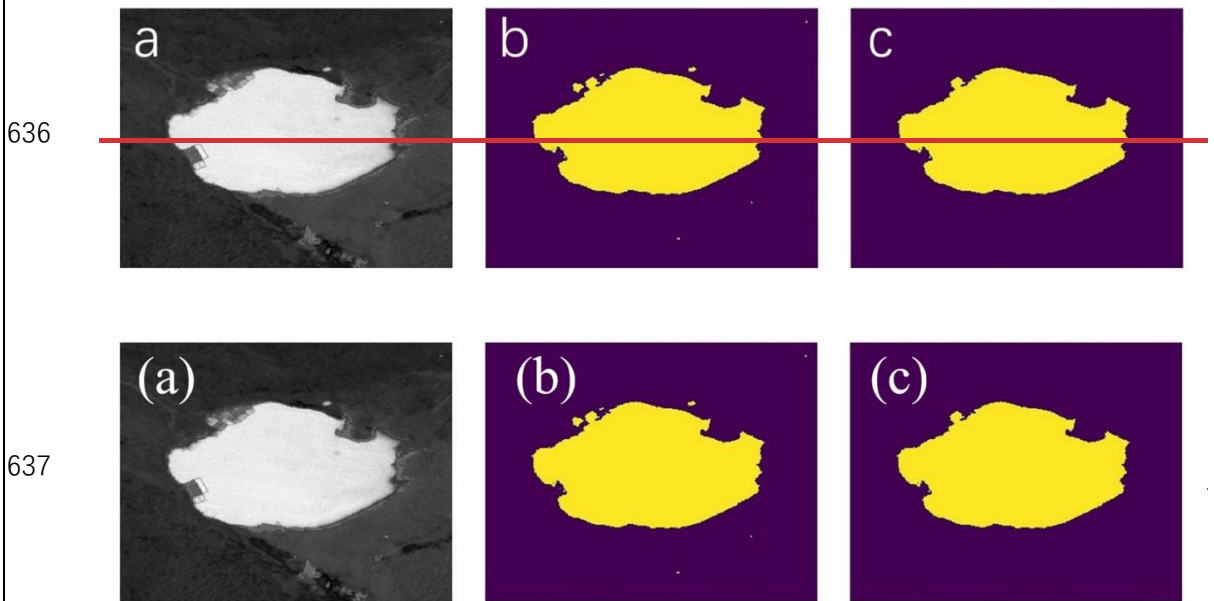
627
$$-$$

628 The lake boundary is extracted using a boundary detection algorithm (e.g., the
629 Canny edge detection algorithm) applied to the selected largest connected region.

630
$$B = \text{Canny}(C_i) \tag{18}$$

631
$$-$$

632 As shown in the ~~figure~~Figure 65, the white areas in the original image include
633 both lakes and buildings. When using threshold segmentation to extract water bodies,
634 buildings may also be mistakenly identified as water. By applying the maximum
635 connected component method, buildings can be effectively separated.



638 Figure 5. Illustration of water extraction and building removal processes. (a) Original Landsat
639 image, in which white areas include both lake water and built-up surfaces; (b) water bodies extracted
640 using threshold-based segmentation; (c) buildings separated from water bodies using the maximum
641 connected component method. Source: Landsat imagery courtesy of the U.S. Geological Survey

642 (USGS), processed and interpreted by the authors. Figure 6: The white areas in the original image
643 include both lakes and buildings (a), water bodies extracted using threshold segmentation (b), and
644 buildings separated using the maximum connected component method (c). Source: Landsat imagery
645 courtesy of the U.S. Geological Survey (USGS), processed and interpreted by the authors.

646 _(8) Cloudy Image Filling Processing

647 3.1.3 Cloudy and striped image reconstruction

648 (1) Cloudy image filling processing

649 The processing steps (5)–(7) are applied to cloud-free images. For cloudy images,
650 cloud-free images are used for filling before executing steps (5)–(7).

651 For cloud-free images, the subsequent water-extraction steps are applied directly.
652 For cloudy images, cloud-free images are first used to reconstruct missing pixels, after
653 which the same processing steps are executed.

654 The filling approach is as follows: Based on the cloud coverage information
655 (CLOUD_COVER), images with cloud cover less than or equal to 30%
656 ($CLOUD_COVER \leq 30\%$) are classified as cloud-free images, while others are
657 considered cloudy images. The formula is as follows:

$$\begin{aligned} \text{Cloudy Image} &= \{\text{Image} \mid CLOUD_{COVER} \leq 30\%\} \\ \text{Cloud-Free Image} &= \{\text{Image} \mid CLOUD_{COVER} > 30\%\} \end{aligned} \tag{19}$$

661 Then, the Mutual Information (MI) algorithm is used to perform the most similar
662 matching between the cloudy image and all cloud-free images. Next, the most similar
663 image is combined with the original cloudy image through a union operation to obtain

664 the filled cloudy image. Finally, the reconstructed images are processed using the same
 665 lake-extraction workflow as applied to cloud-free images, producing the final water-
 666 body area estimates ~~Finally, steps (5)–(7) from the cloud-free image processing are~~
 667 ~~executed, resulting in the final water body area. The specific steps are as follows:~~

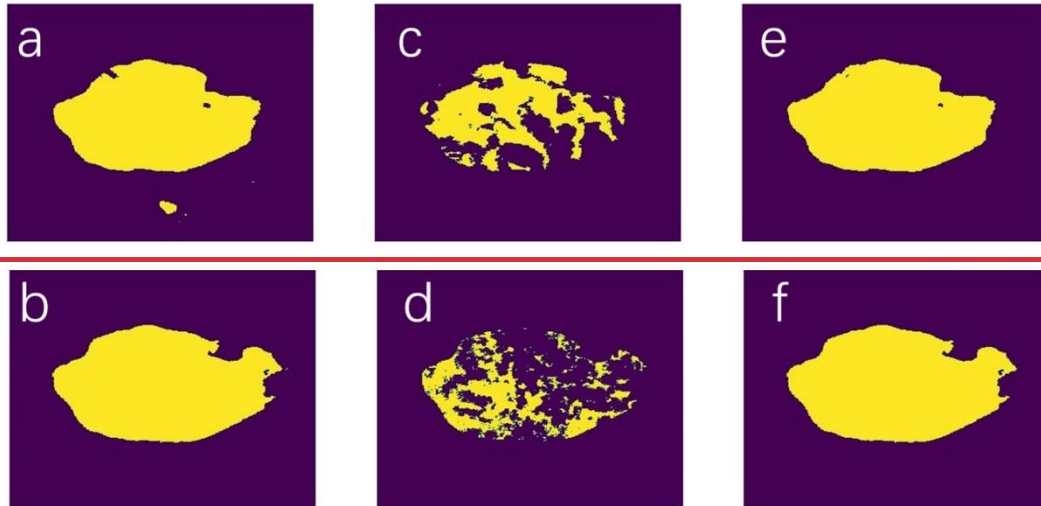
668 Candidate Cloud-Free Image Set: In the time periods before and after the cloudy
 669 image, select images with low cloud coverage ($\text{CLOUD_COVER} \leq 30\%$) as the
 670 candidate image set.

671 Mutual Information Algorithm: Use the MI algorithm to calculate the similarity
 672 between the cloudy image and the candidate cloud-free images. The formula is as
 673 follows:

$$674 \quad I(I_{cloudy}, I_{clear}) = \sum_{i,j} p(I_{cloudy} = i, I_{clear} = j) \log \left(\frac{p(I_{cloudy} = i, I_{clear} = j)}{p(I_{cloudy} = i) p(I_{clear} = j)} \right) \quad (20)$$

676 Where I_{cloudy} represents the cloudy image, I_{clear} represents the candidate cloud-
 677 free image, and P is the joint probability distribution of the pixel grayscale values. I
 678 denotes mutual information, which measures the correlation between the cloudy image
 679 and the cloud-free image.

680 Selecting the Most Similar Image: Based on the mutual information value, the
 681 cloud-free image most similar to the cloudy image is selected.

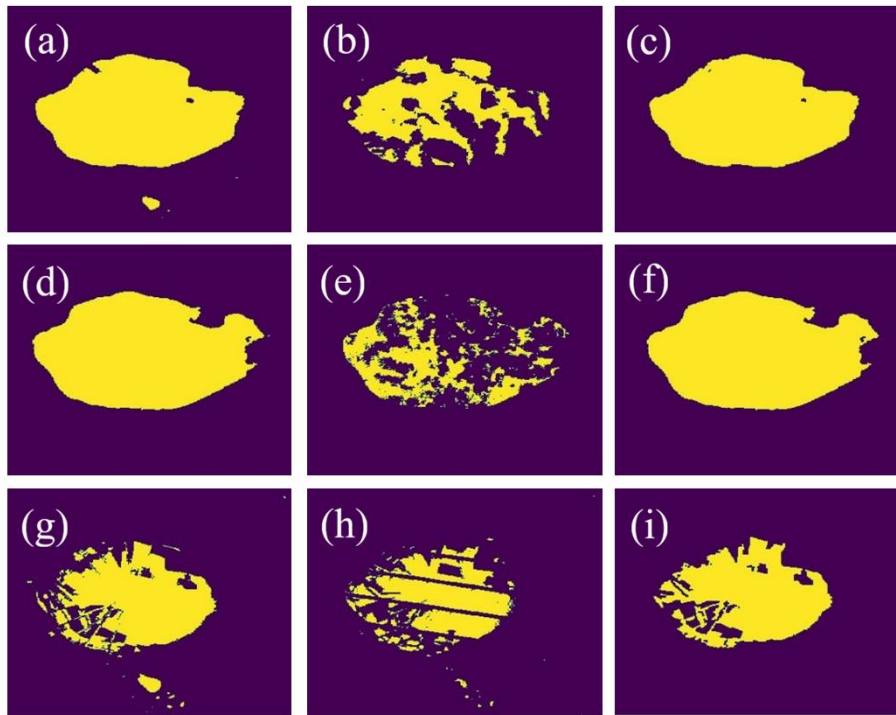


682
 683 ~~Figure 7: Image a and b show the cloud-free images found to be most similar to~~
 684 ~~the cloudy images images c and d are the cloudy images, and images e and f show the~~
 685 ~~result after cloud-filled processing of the cloudy images. Source: Landsat imagery~~
 686 ~~courtesy of the U.S. Geological Survey (USGS), processed and interpreted by the~~
 687 ~~authors.~~

688 (2) Striped image filling (9) Striped Image Filling

689
 690 The previously mentioned dataset indicates that Landsat 7 TM images have
 691 significant striping interference. Additionally, Landsat 5 TM and Landsat 8 OLI images
 692 also experience striping interference in certain months, such as Landsat 5 TM from
 693 2001 to 2003 and Landsat 8 in 2008. To more accurately obtain the temporal changes
 694 in lake area, it is necessary to fill the missing portions of striped images. The method is
 695 the same as for cloud-filled images. By utilizing the clear contours of historical cloud-
 696 free images and applying the MI algorithm, the most similar historical cloud-free
 697 images are searched to fill the water pixels in the striped regions. The method for filling

698 striped images is the same as that for cloud-filled images. ~~Afterward, steps (5)–(7) are~~
699 ~~executed to obtain the final water area extent.~~



701 Figure 6: Filling processing of cloudy and striped-interference lake images using similar cloud-
702 free references. (a)\(d) Cloud-free reference images identified as most similar to the cloudy images;
703 (b)\(e) Original cloudy images;(c)\(f) Cloud-filled results after processing; (g) Cloud-free image
704 most similar to the striped-interference image;(h) Original striped-interference image;(i) Result after
705 stripe-filling processing. Source: Landsat imagery courtesy of the U.S. Geological Survey (USGS),
706 processed and interpreted by the authors.



708 Figure 7: Image a and b show the cloud-free images found to be most similar to the
709 cloudy images images c and d are the cloudy images, and images e and f show the result

710 after cloud filled processing of the cloudy images. Source: Landsat imagery courtesy
711 of the U.S. Geological Survey (USGS), processed and interpreted by the authors.

712 ~~Figure 8: The image found from the cloud free images that is most similar to the striped~~
713 ~~interference image (a); The striped interference image(b); The effect after filling the~~
714 ~~striped interference(c). Source: Landsat imagery courtesy of the U.S. Geological~~
715 ~~Survey (USGS), processed and interpreted by the authors.~~

716 ~~(10) 3.1.4 Monthly synthesis and time-series construction~~ Water Area Extraction

717 After applying the maximum connectivity component processing to the image, the
718 number of water pixels is counted. Then, based on the spatial resolution of the pixels
719 (30m * 30m), the actual area is calculated.

720 ~~(11) Interpolation Processing~~

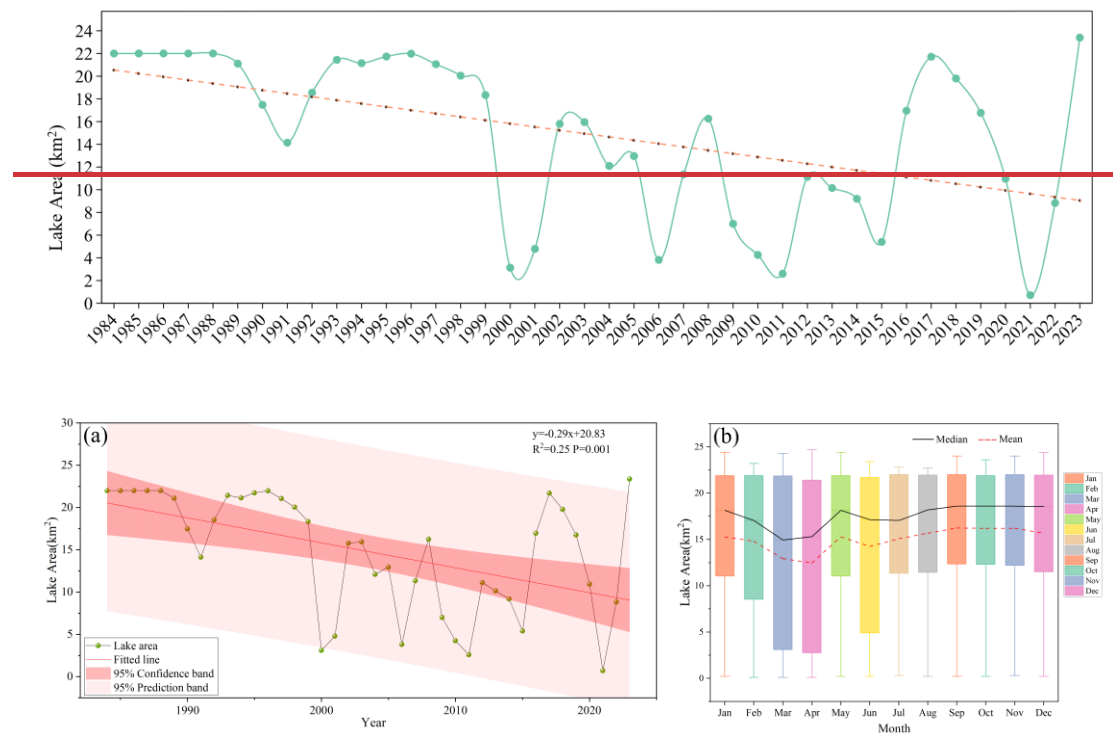
721 Collect all known lake area data for specific time points, where t_i dots represent
722 time points with available data. For each missing data point t_{missing} , use the known data
723 points $t_{\text{missing}-1}$ and $t_{\text{missing}+1}$, and apply the selected interpolation method to calculate
724 the lake area $A(t_{\text{missing}})$ at time.

725 ~~3.2 Lake Area-area Time-time Series-series Construction~~ Construction

726 ~~3.2.1 Monthly lake-area time series and seasonal variability of Bahannao Lake~~

727 The interannual variation of Bahannao is quite drastic, but the overall trend is
728 declining (Figure 7(a)), linear regression analysis based on the year index reveals a
729 significant declining trend in the lake area from 1984 to 2024, with a decrease rate of
730 -0.29 km² yr⁻¹ (p = 0.001). The coefficient of determination (R² = 0.25) indicates
731 substantial interannual variability, suggesting that although the long-term trend is

732 statistically robust, short-term fluctuations and nonlinear processes play an important
 733 role in shaping lake-area dynamics~~though not significantly~~. Before 1999, the changes
 734 were relatively stable. In 2000, the lake area shrank severely, decreasing by 82.98%
 735 compared to 1999, leaving only 3.12 km². Since then, the lake has exhibited a cyclical
 736 fluctuation pattern with a period of approximately 5–6 years. In 2021, the lake area
 737 reached its minimum value of just 0.71 km², followed by a rapid increase, reaching its
 738 maximum of 23.38 km² in 2023.



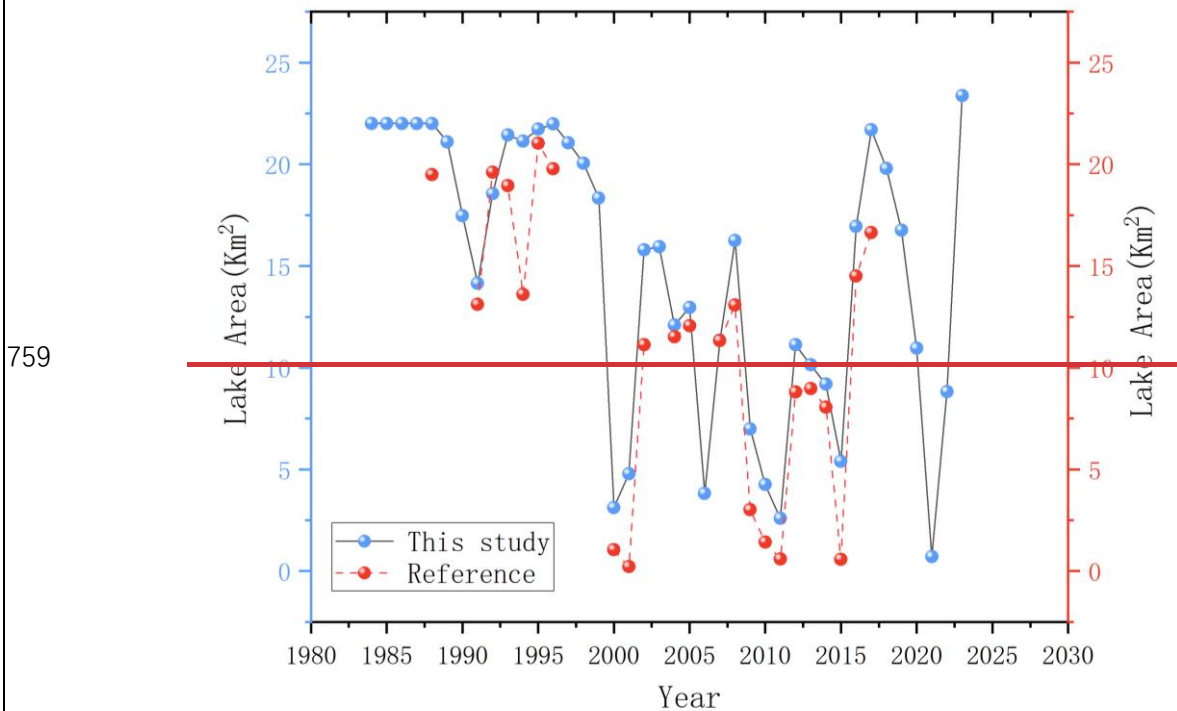
741 Figure 9-7 Interannual and intra-annual ~~V~~variation of Bahannao Lake-Lake Areaarea. (a)
 742 Interannual variations of lake area; (b) multi-year mean monthly variations of lake area.

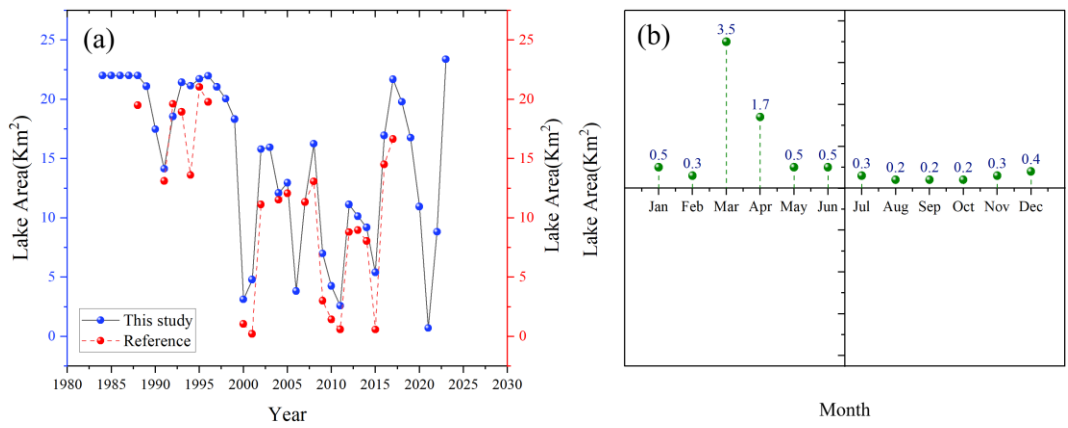
743 Due to its location in the Mu Us Desert and the lack of long-term observational
 744 data, this study references the lake area interpreted via remote sensing in the
 745 *Comprehensive Lake Water Ecological Management Plan of Uxin Banner*. This report
 746 provides remote sensing imagery data for 24 years from 1988 to 2018 (with six years

747 lacking clear images suitable for analysis).

748 A comparison of the data (Figure 108(a)) shows that the lake area interpreted in
749 this study aligns with the trend reported in the management plan. Over the 23 years of
750 overlapping interpretation, the error remains within 15% for 12 years. However, in
751 years when the lake area was smaller, the error was relatively larger, such as in 2000,
752 2001, 2009, 2010, 2011, and 2015. According to records, Bahannao Lake shrank
753 significantly during these years but did not completely dry up until 2021, which is
754 consistent with the results of this study.

755 The interpreted lake area in this study also indicates (Figure 8(b)) that the annual
756 average area of Bahannao Lake in 2021 was only 0.71 km². The lake area was at its
757 smallest in August, September, and October, reaching only 0.2 km², while the largest
758 area was recorded in March at 3.5 km².



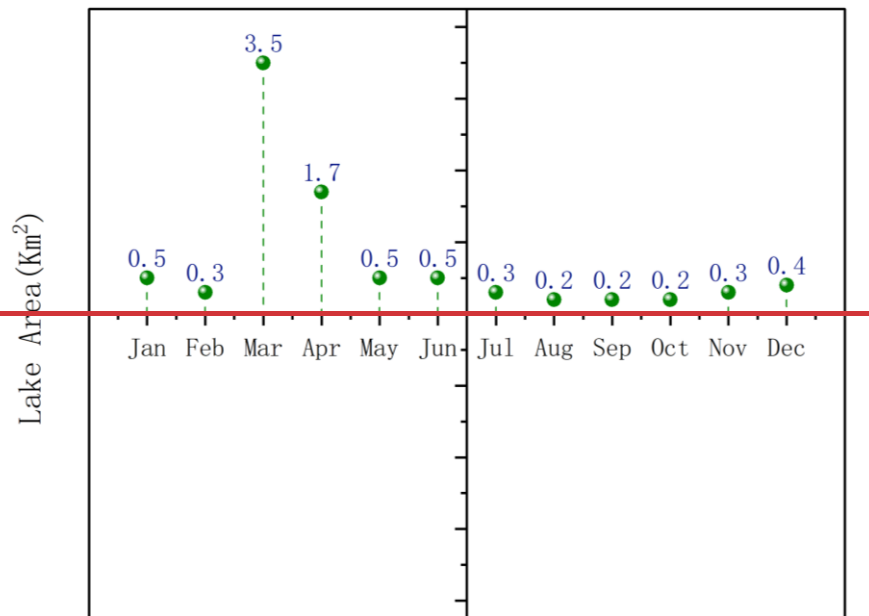


761 Figure 8 Validation of lake area estimates and intra-annual variability in a typical year (2021).

762 (a) Comparison between lake area derived in this study and reference datasets;(b) monthly variations
 763 of lake area in 2021, selected as a representative year to illustrate intra-annual dynamics.

764 Figure 10 Comparison of the lake area interpreted in this study with the reference

765 data



766 Figure 11 Monthly and seasonal variation of lake area in 2021

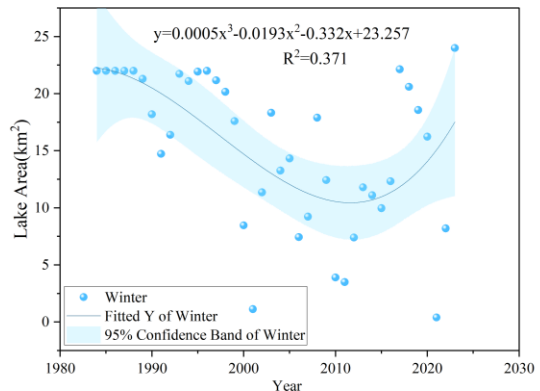
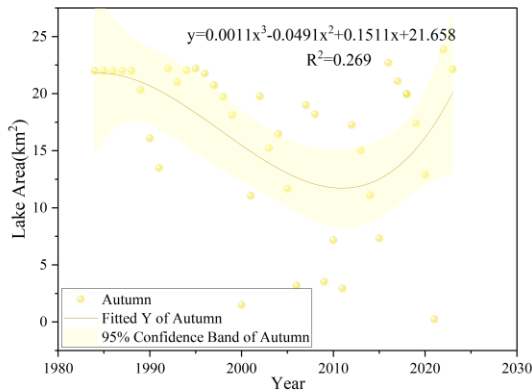
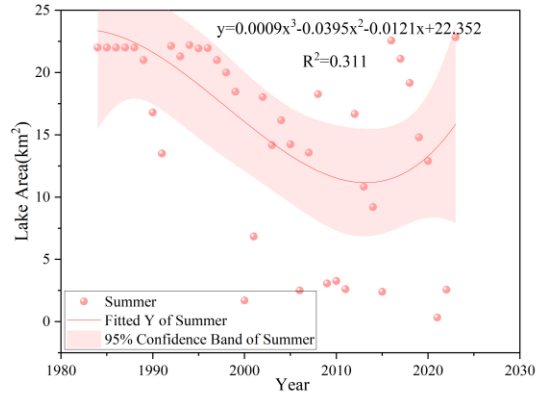
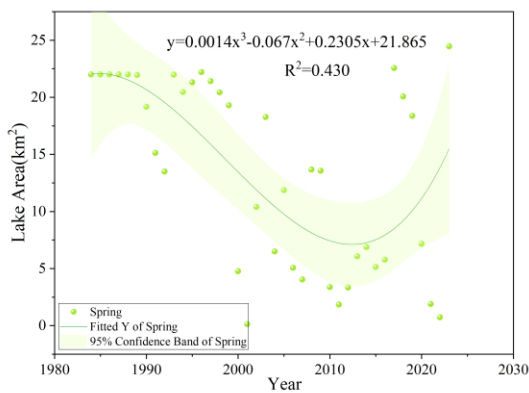
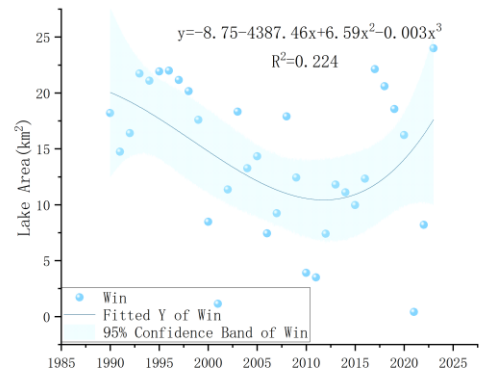
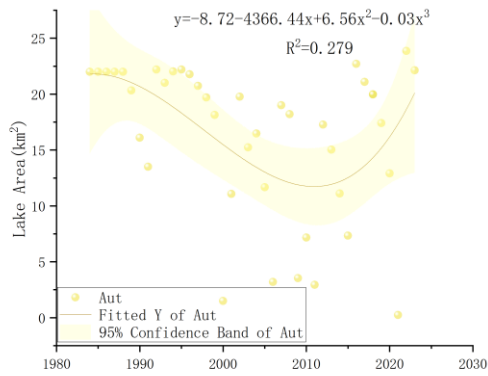
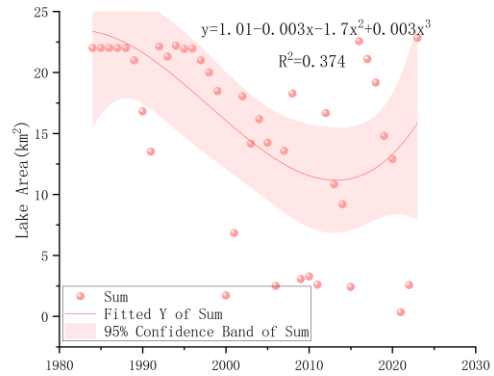
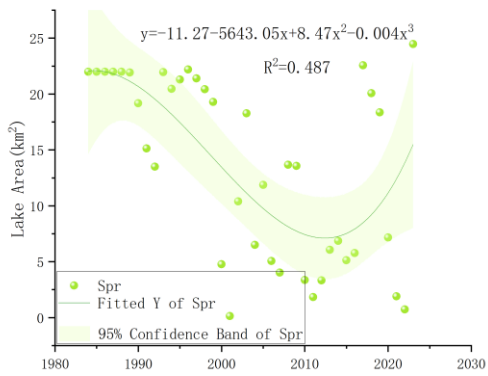
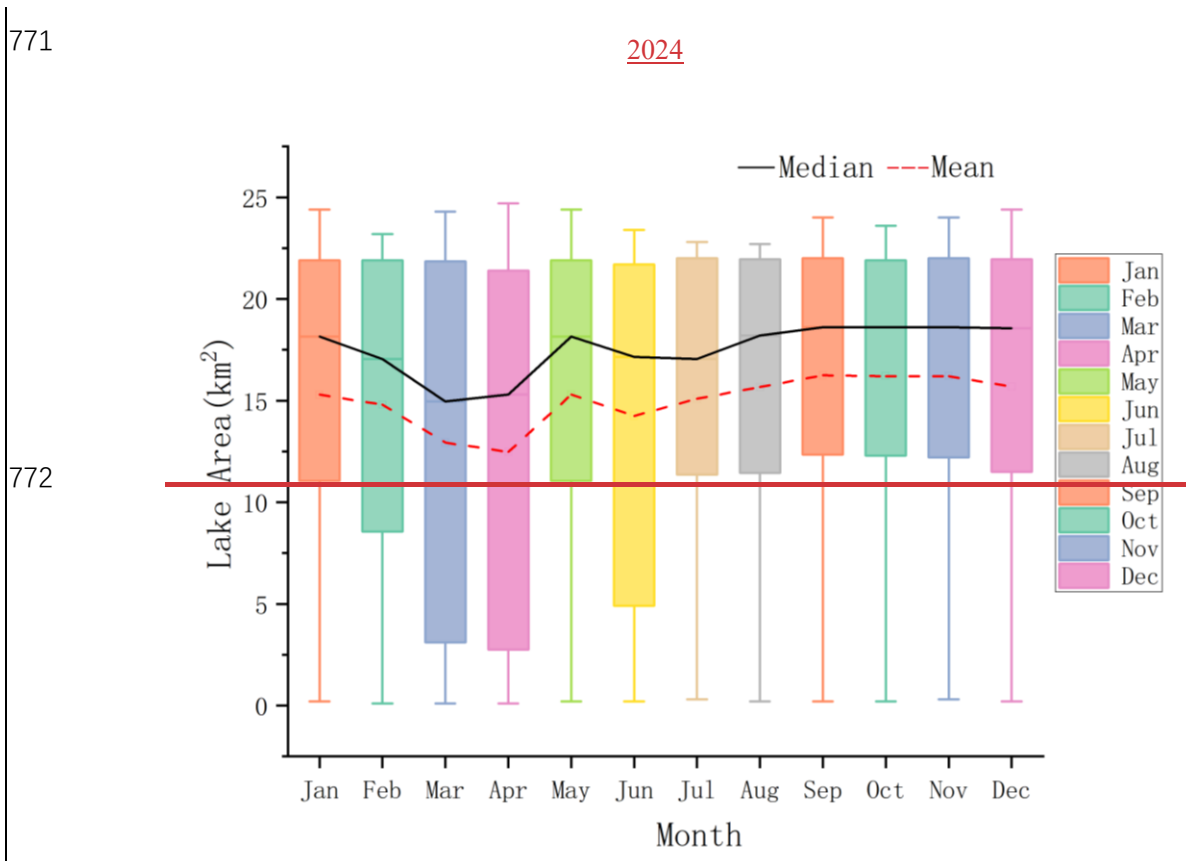


Figure 12-9 Seasonal Variation-variation of Lake-lake Area-area during the period of 1984-



773 Figure 13 Monthly Variation of Lake Area

774 From the perspective of seasonal (Figure 9) and monthly (Figure 7(b)) variation

775 characteristics, Bahannao exhibits significant seasonal differences. The lake area in

776 summer, autumn, and winter is noticeably larger than in spring, with autumn having the

777 largest lake area, averaging 16.21 square kilometers and reaching a peak of 16.24 square

778 kilometers in September. In contrast, spring has the smallest lake area, averaging only

779 13.57 square kilometers, with the lowest value of 12.48 square kilometers occurring in

780 April.

781 3.2.2 Method validation using representative lakes in arid regions

782 To further evaluate the robustness and regional applicability of the proposed lake-

783 area extraction method, we applied the same remote-sensing workflow to two

784 representative lakes in arid and semi-arid northern China: Hongjiannao Lake and

785 Wuliangshuai Lake. These lakes differ markedly in size, hydrological conditions, and
786 degree of human influence, and have been widely investigated in previous remote-
787 sensing studies, providing independent reference datasets for method validation.

788 Using the identical image-processing procedures and water-body extraction
789 criteria as those employed for Bahannao Lake, we constructed annual lake-area time
790 series for both Hongjiannao Lake and Wuliangshuai Lake (Figure 10). The derived time
791 series capture the major interannual fluctuations and long-term trends of lake-area
792 variability for both lakes.

793 To quantitatively assess consistency with existing studies, the lake-area estimates
794 obtained in this study were compared with previously published lake-area datasets
795 (Figure 11). For both lakes, the temporal evolution and long-term trends derived in this
796 study show good agreement with reference datasets reported in the literature.

797 For Hongjiannao Lake, quantitative comparison indicates that the relative
798 differences between lake-area estimates derived in this study and published datasets
799 generally remain within a reasonable range. Specifically, the maximum and minimum
800 relative differences are 14.65% and 9.12% when compared with Ji et al. (2023), 18.70%
801 and 9.57% with Xie et al. (2021), 11.82% and 8.29% with Ma et al. (2020), 11.30% and
802 7.94% with Wang et al. (2018), and 10.57% and 3.15% with Liu et al. (2016).

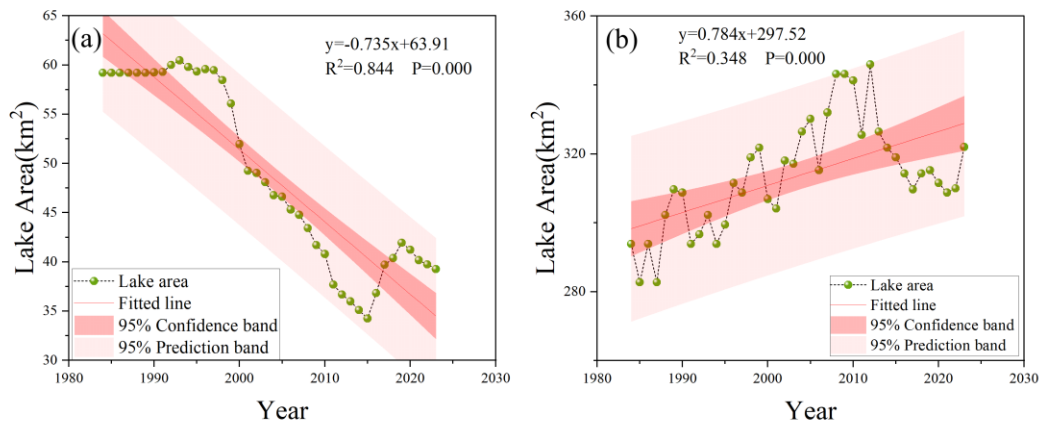
803 For Wuliangshuai Lake, the relative differences are generally smaller, with
804 maximum differences of 8.50% (minimum 1.74%) compared with Guan et al. (2022),
805 8.02% (minimum 1.79%) compared with Li et al. (2023), and 18.12% (minimum 1.09%)
806 compared with Tan et al. (2021). These results indicate a high level of consistency

807 between the lake-area estimates derived in this study and those reported in previous
808 literature.

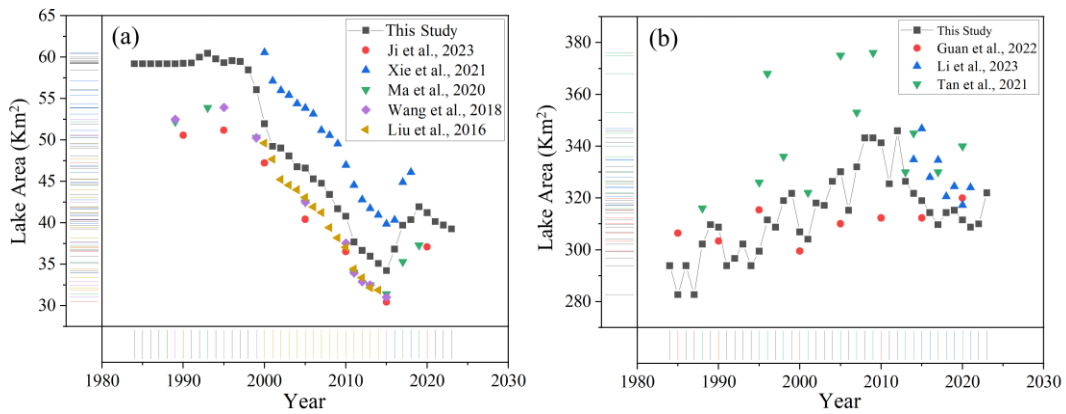
809 Although minor discrepancies in absolute lake-area values are observed, these
810 differences can be attributed to variations in image selection, water-index thresholds,
811 temporal coverage, and post-processing strategies among different studies. An
812 additional source of discrepancy arises from differences in temporal aggregation
813 strategies. In this study, annual lake area is calculated as the mean of monthly lake-area
814 estimates derived from all available images within a year, which reduces the influence
815 of short-term fluctuations and image-specific noise. In contrast, many previous studies
816 report lake area based on a single image or a limited number of images selected for each
817 year. Such differences in temporal representation can lead to systematic deviations in
818 absolute lake-area values, particularly for lakes exhibiting strong intra-annual
819 variability.

820 Overall, the consistency between our results and independent reference datasets
821 supports the robustness and transferability of the proposed lake-area extraction method
822 across different lake types in arid and semi-arid regions. This validation provides
823 confidence that the method is suitable for long-term lake-area monitoring and
824 comparative analysis in data-sparse dryland environments.

825



826
827 Figure 10 Interannual variations in lake area for Hongjiannao Lake (a) and
828 Wuliangshuai Lake (b).



829
830 Figure 11 Comparison of lake area estimates derived in this study with published reference
831 datasets. (a) Comparison of Hongjiannao Lake area with lake-area estimates reported in previous
832 studies; (b) Comparison of Wuliangshuai Lake area with lake-area estimates reported in previous
833 studies.

834 3.3 Impact of Climate-climate Changechange

835 3.3.1 Changes of hydro-climate series

836 (1) Temperature and moisture conditionsTemperature Variation

837 1) Temperature and 2m dew point temperature

838 The rise in air temperature directly affects the evaporation rate of the lake. The

warming rate is $0.0429043^{\circ}\text{C yr}^{-1}$ (Figure 12(a)) per year, leading to an increase in the lake surface temperature and, consequently, higher evaporation. High temperatures intensify water evaporation, reducing the lake's water volume and causing a gradual decrease in lake area over the years.

The increase in air temperature enhances heat input into the water body, accelerating evaporation. As more heat is absorbed, surface water transforms more easily into water vapor, leading to a decline in lake water levels. Although the influence of temperature on lake area varies across different time periods, its continuous upward trend has a long-term impact on the reduction of lake area.

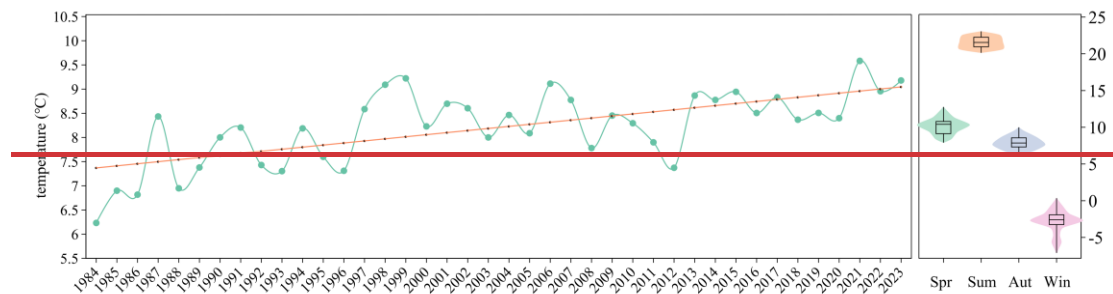
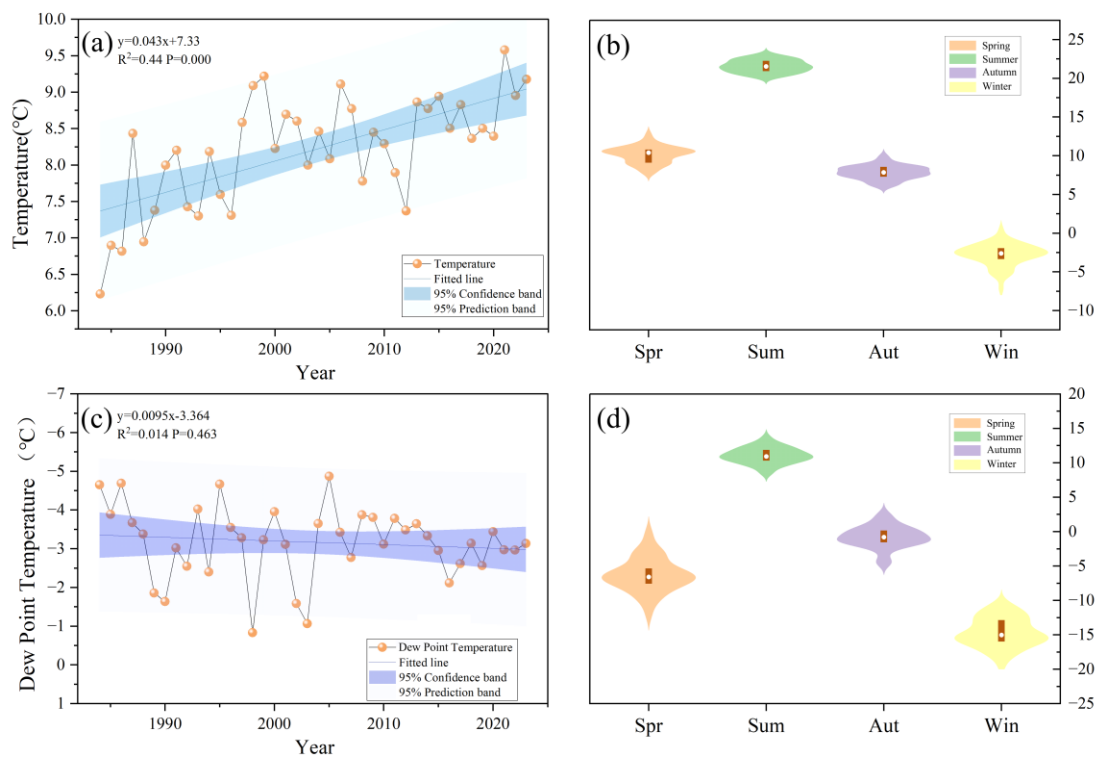


Figure 14 Regional Air Temperature Variation

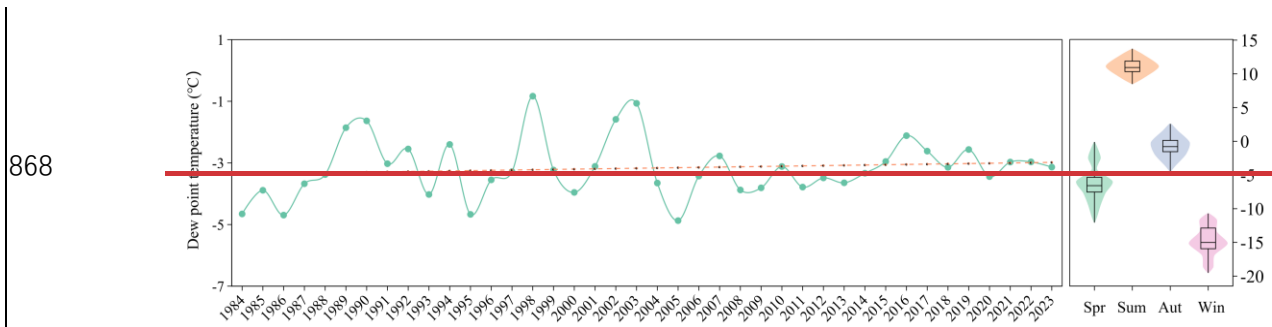
2) 2m Dew Point Temperature

The 2m dew point temperature increases at a rate of $0.0095^{\circ}\text{C yr}^{-1}$ (Figure 12(c)) a, indicating changes in atmospheric humidity. A rising dew point temperature suggests an increase in water vapor content in the air, typically associated with higher humidity. However, humidity changes do not always directly impact lake area; instead, they influence lake water volume indirectly by affecting evaporation and precipitation. While an increase in dew point temperature usually indicates higher humidity, if

858 precipitation is insufficient or evaporation rates are too high, this increase in humidity
 859 may not effectively replenish lake water. Instead, it could contribute to lake shrinkage.
 860 The varying influence of the 2m dew point temperature over different periods suggests
 861 a complex relationship with lake area changes, requiring a comprehensive analysis
 862 alongside other climatic factors.



863
 864 Figure 12 Temporal and seasonal variations in air temperature and 2 m dew point temperature
 865 over the study area during the period of 1984-2024 ((a) Interannual variations in air temperature; (b)
 866 Multi-year mean seasonal cycle of air temperature;(c) Interannual variations in 2 m dew point
 867 temperature;(d) Multi-year mean seasonal cycle of 2 m dew point temperature)



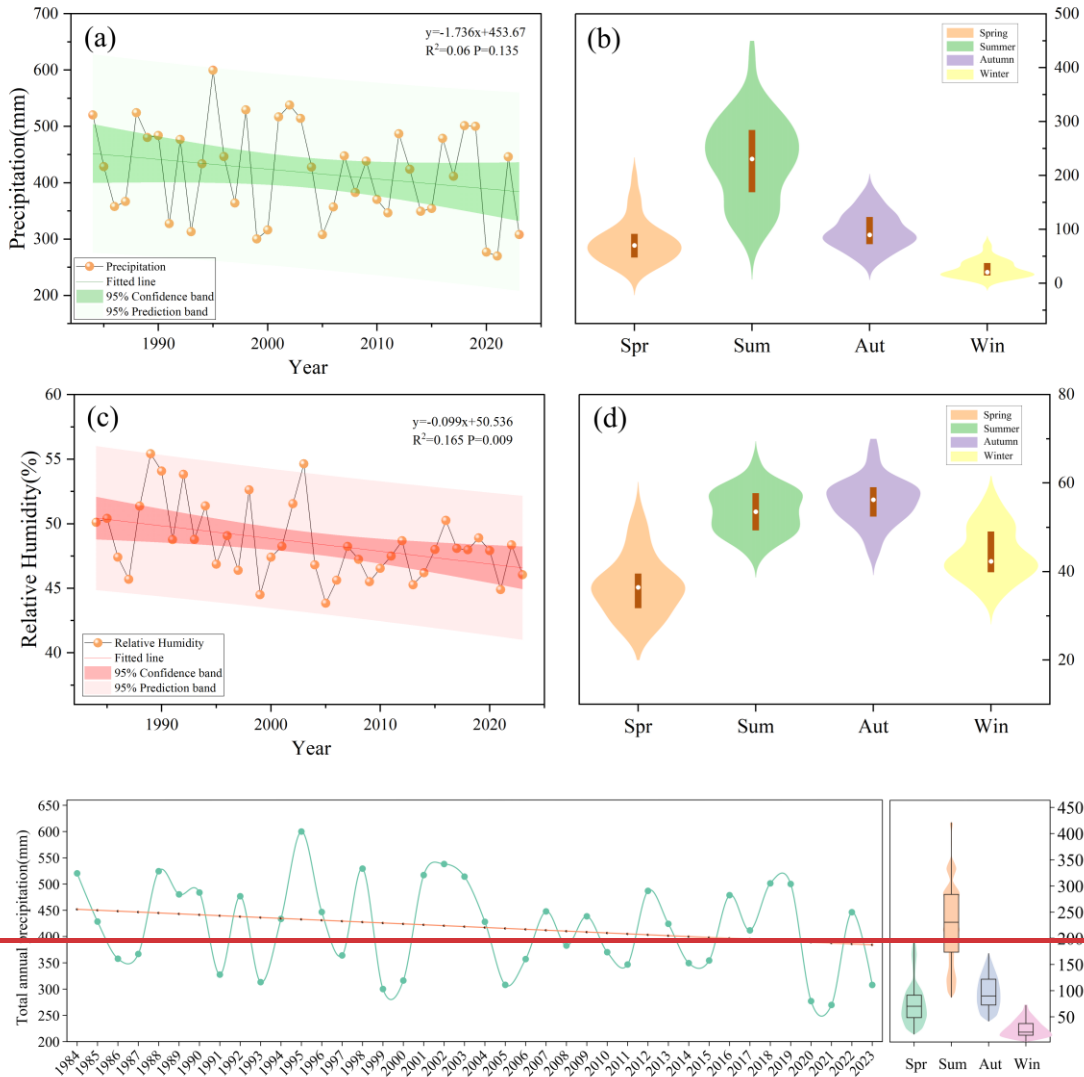
868 **Figure 15 Regional 2m Dew Point Temperature Changes**

869 **(22) Changes in Precipitation and relative humidity**

870 The total precipitation is decreasing at a rate of $1.7355-736 \text{ mm yr}^{-1}$ (Figure
 871 13(a))per year. Precipitation is one of the primary sources of lake water. A reduction in
 872 precipitation leads to insufficient water replenishment for the lake, resulting in a decline
 873 in water levels and a reduction in lake area.

874 **1) Relative Humidity**

875 The relative humidity decreases at a rate of 0.09879 yr^{-1} (Figure 13(c))per year. A
 876 decrease in humidity typically accelerates evaporation from the lake, leading to a
 877 reduction in lake area. The decrease in humidity means that the air becomes drier, and
 878 the evaporation rate increases. This accelerates the evaporation of lake water, resulting
 879 in a decline in both lake water levels and area, intensifying the process of lake
 880 desiccation.



882

883

884

885

886

887

888

889

890

891

892

Figure 13 Temporal and seasonal variations in precipitation and relative humidity over the study area during the period of 1984-2024 ((a) Interannual variations in precipitation; (b) Multi-year mean seasonal cycle of precipitation;(c) Interannual variations in relative humidity;(d) Multi-year mean seasonal cycle of relative humidity)

Figure 16 Regional Precipitation Changes

(32) Surface radiation and heat flux components Radiation and Energy Exchange

1 → Net Longwave-longwave Radiation-radiation and net shortwave radiation at the Surfaesurface

Net longwave radiation at the surface decreases by $0.0843 \text{ W/m}^2 \text{ yr}^{-1}$ (Figure

893 14(a))per year. The reduction in longwave radiation means that the lake receives less
 894 radiative heat, which theoretically could reduce evaporation. However, this effect is
 895 overshadowed by other factors such as reduced precipitation and rising temperatures.
 896 While the decrease in longwave radiation could reduce heat loss from the lake, in
 897 conditions of drought and high evaporation, the impact of this reduction is likely limited.

898 2) Net Shortwave Radiation at the Surface

899 Net shortwave radiation at the surface increases by $0.0653 \text{ W/m}^2 \text{ yr}^{-1}$ (Figure
 900 14(a))per year. The increase in shortwave radiation enhances the evaporation process,
 901 thereby reducing the lake's surface area. The rise in shortwave radiation leads to an
 902 increase in surface temperature, which accelerates evaporation. The intensified
 903 evaporation exacerbates the loss of water from the lake. The effect of increased
 904 shortwave radiation on the lake's area is significant during all periods, especially under
 905 drought and high-temperature conditions, where its impact is particularly pronounced.

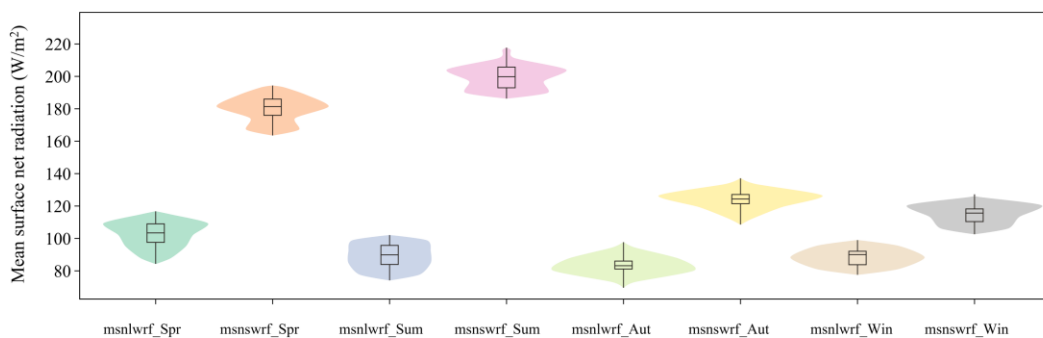
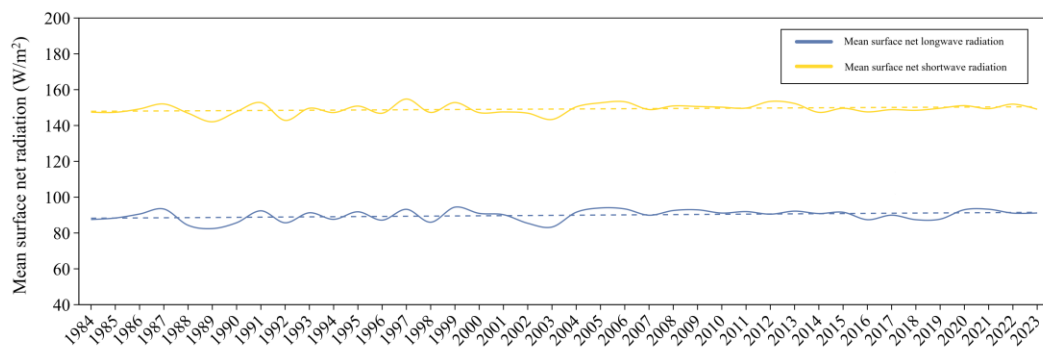


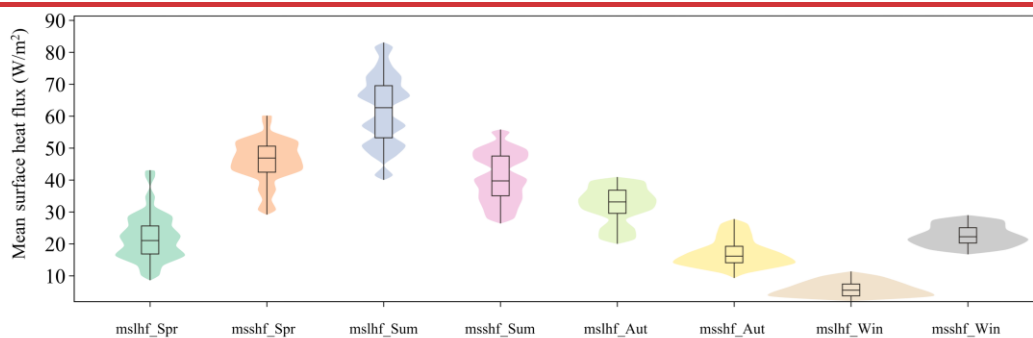
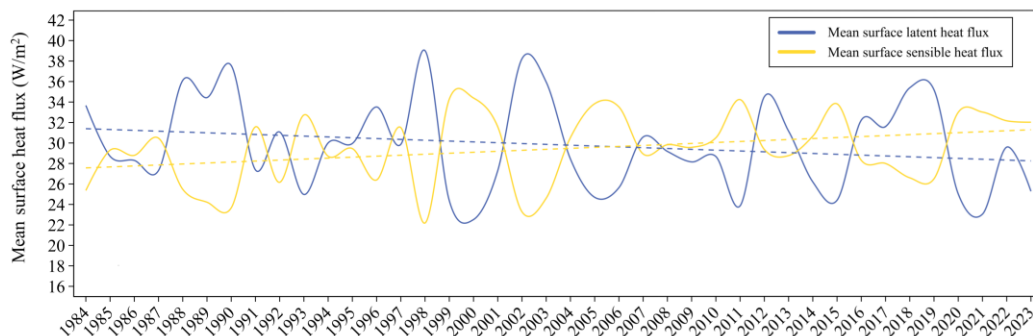
Figure 17 Regional Mean Surface Net Radiation

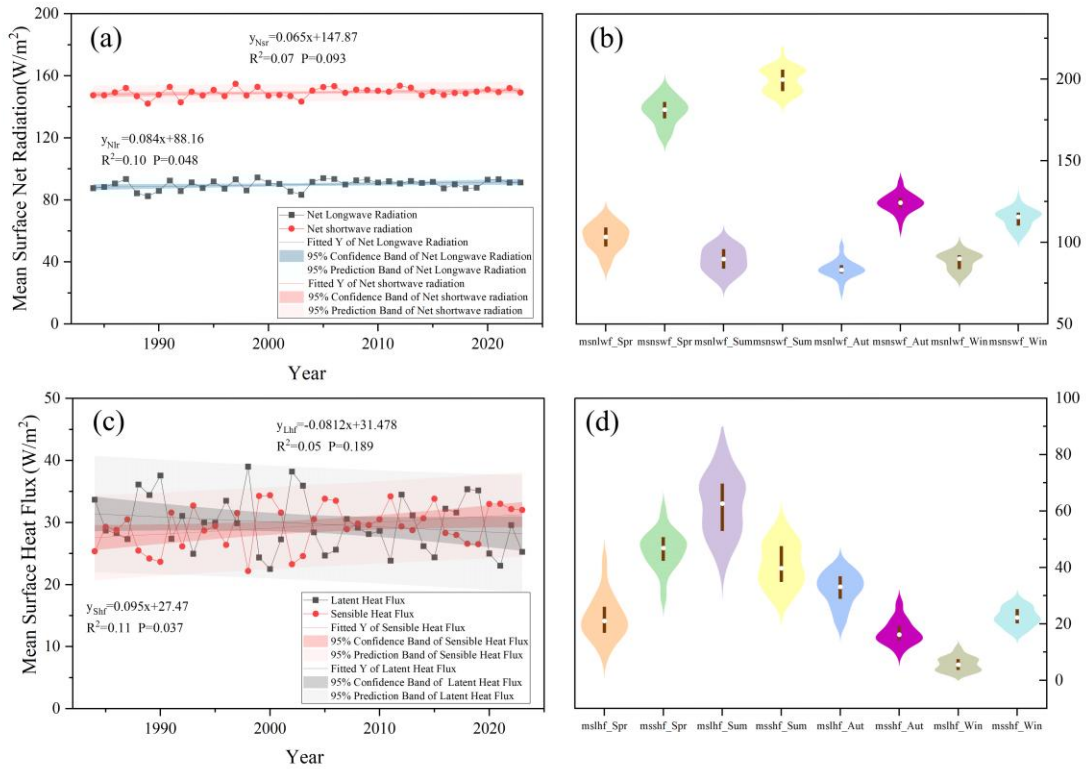
32) Mean Surface Latent Heat Flux and sensible heat flux

The latent heat flux decreases at a rate of $0.1343-081 \text{ W/m}^2 \text{ yr}^{-1}$ (Figure 14(c)) per year. The decrease in latent heat flux indicates a reduction in the moisture carried by the air, possibly as a result of decreased humidity, which further intensifies evaporation from the water.

4) Mean Surface Sensible Heat Flux

The sensible heat flux increases by $0.0693-095 \text{ W/m}^2 \text{ yr}^{-1}$ (Figure 14(c)) per year, meaning that the heat exchange between the surface and the atmosphere is enhanced. This leads to more evaporation, particularly during the summer when temperatures are higher.





919

920

Figure 18-14 Regional variations of surface net radiation and surface heat flux during 1984 -

921

2024. (a) Interannual variations of mean surface net radiation; (b) multi-year mean seasonal

922

variations of surface net radiation; (c) interannual variations of mean surface heat flux; (d) multi-

923

year mean seasonal variations of surface heat flux.~~Regional Mean Surface Heat Flux~~

924

Abbreviations: msnlwf denotes mean surface net longwave radiation; mnsnwf denotes mean

925

surface net shortwave radiation; mslhf denotes mean surface latent heat flux; msshf denotes mean

926

surface sensible heat flux. The suffixes Spr, Sum, Aut, and Win represent spring, summer, autumn,

927

and winter, respectively.

928

(3) Evaporative demand and aridity conditions

929

(41) Humidity and Potential evapotranspiration~~Evapotranspiration~~

930

1) Relative Humidity

931

The relative humidity decreases at a rate of 0.0987 per year. A decrease in humidity

typically accelerates evaporation from the lake, leading to a reduction in lake area. The decrease in humidity means that the air becomes drier, and the evaporation rate increases. This accelerates the evaporation of lake water, resulting in a decline in both lake water levels and area, intensifying the process of lake desiccation.

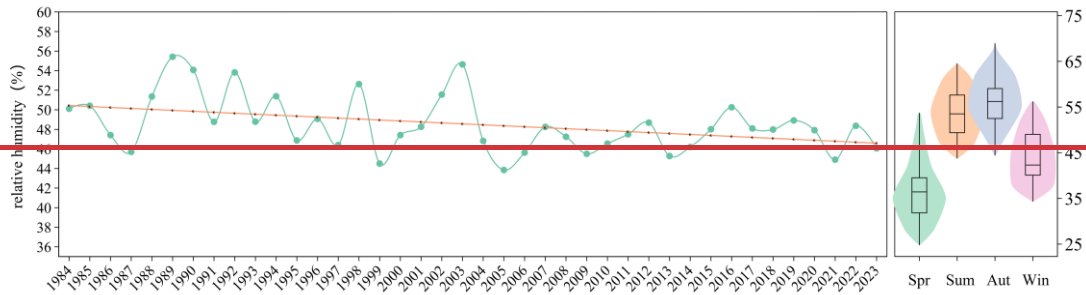
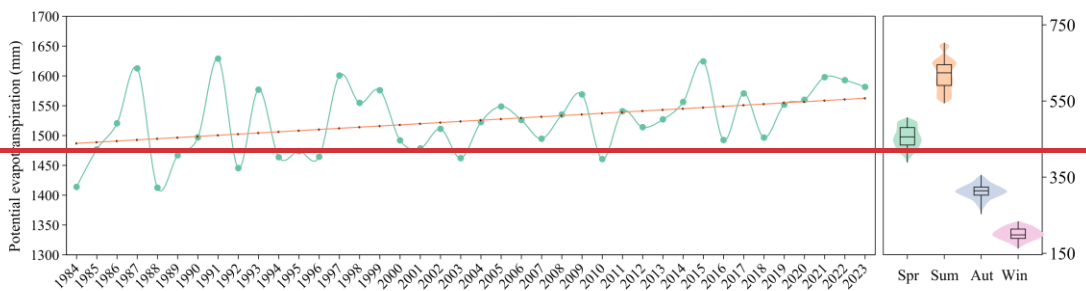


Figure 19 Regional Relative Humidity

2) Potential Evapotranspiration

Potential evapotranspiration increases at a rate of 1.9369-937 mm yr⁻¹ (Figure 15(a)) per year. The increase in evapotranspiration directly leads to the loss of water from the lake, making it an important factor contributing to the reduction in lake area. The rise in potential evapotranspiration indicates that both evaporation and plant transpiration in the lake area are increasing, further reducing the water volume of the lake. The increase in potential evapotranspiration has a significant impact on the lake area in all time periods, especially under drought and high-temperature conditions, where its effect is even more pronounced.



948 **Figure 20 Regional Potential Evapotranspiration**

949 **(52) Drought**

950 The aridity index (AI) exhibits pronounced interannual variability over the study
951 period, with values generally fluctuating between approximately 0.18 and 0.40 (Figure
952 15(c)), indicating persistently dry climatic conditions in the study area. Although a
953 decreasing trend is observed (-0.0015 yr^{-1}), the trend is not statistically significant at
954 the 0.05 level ($p = 0.07$), suggesting that long-term aridity intensification is moderate
955 rather than abrupt.

956 Despite the weak linear trend, the consistently low AI values (< 0.5) confirm that
957 Bahannao Lake is located within a semi-arid to arid climatic regime, where water
958 availability is inherently limited and highly sensitive to changes in hydro-climatic
959 forcing. The wide prediction band further reflects strong year-to-year variability in
960 regional moisture conditions, likely driven by fluctuations in precipitation and
961 evaporative demand.

962 Importantly, the combination of a marginally decreasing AI trend and a
963 significant increase in potential evapotranspiration implies a gradual shift toward
964 enhanced atmospheric water demand, even in the absence of a statistically significant
965 drying trend in AI alone. This suggests that lake-area dynamics are more strongly
966 controlled by evaporative processes than by precipitation-driven moisture supply,
967 particularly in recent decades. The drought index decreases at a rate of 0.0019 per year,
968 indicating that the drought conditions in the region are intensifying, further contributing
969 to the shrinkage of the lake.

970

971 In addition to interannual variability, the aridity index (AI) exhibits pronounced
972 seasonal contrasts (Figure 15(d)). Summer shows the highest AI values, with a
973 relatively wide distribution and higher median, indicating comparatively wetter
974 conditions driven by concentrated precipitation during the warm season. Autumn
975 presents intermediate AI values, reflecting a transition from moisture input to increasing
976 evaporative demand.

977 In contrast, spring and winter are characterized by distinctly lower AI values.
978 Spring exhibits low median AI and limited dispersion, indicating persistent moisture
979 deficit during the lake recharge period. This seasonal dryness coincides with rising
980 temperatures and increasing evaporative demand, which constrains lake expansion
981 despite episodic precipitation events. Winter shows the lowest AI values overall,
982 reflecting extremely dry atmospheric conditions dominated by minimal precipitation
983 and suppressed moisture availability.

984 The seasonal pattern of AI highlights that Bahannao Lake is subject to strong intra-
985 annual asymmetry in hydro-climatic conditions, with relatively favorable moisture
986 supply confined to summer, while prolonged dry conditions prevail during spring and
987 winter. Such seasonal dryness amplifies the sensitivity of lake area to evaporative
988 processes.

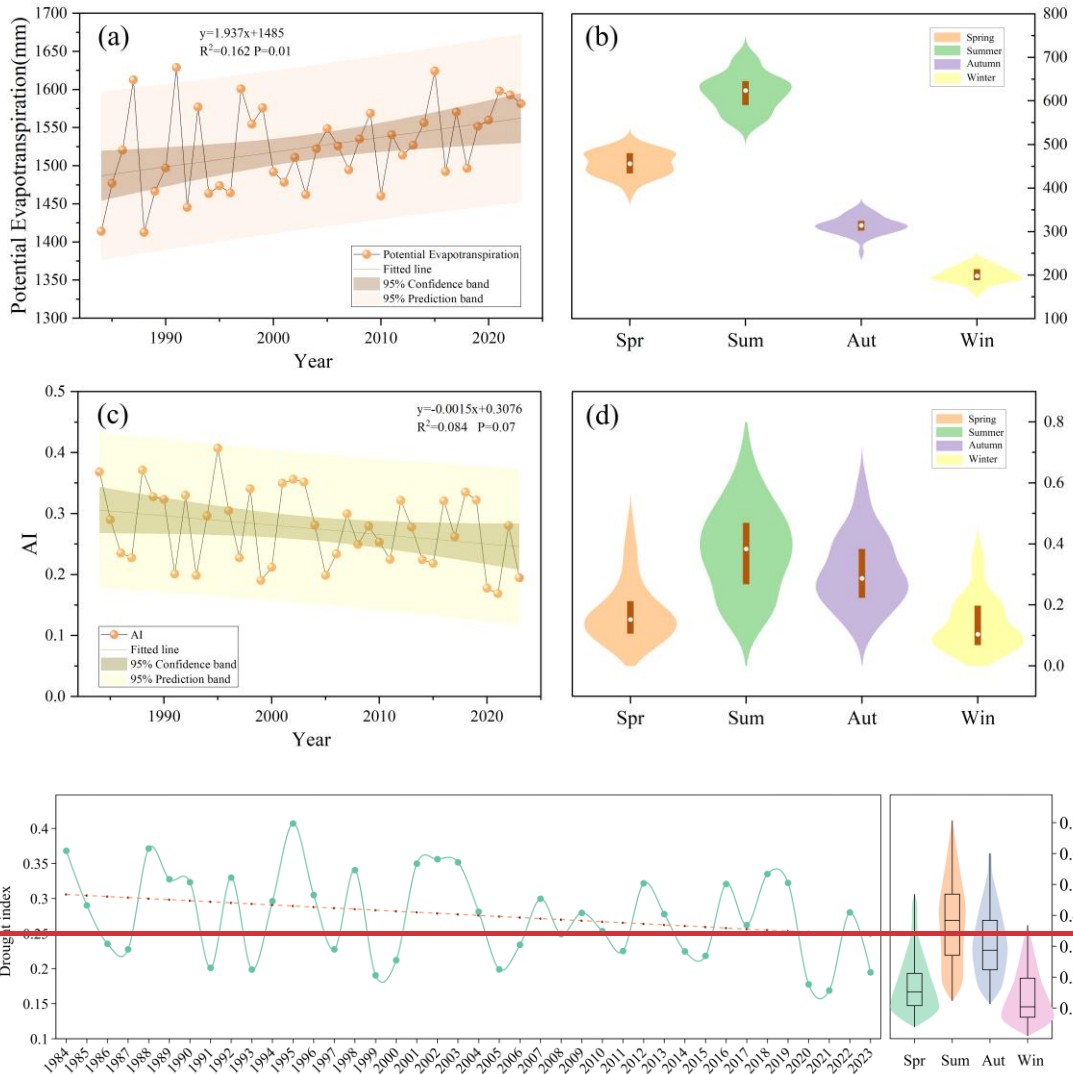


Figure 21-15 Regional variations in evaporation and drought conditions during 1984 - 2024.

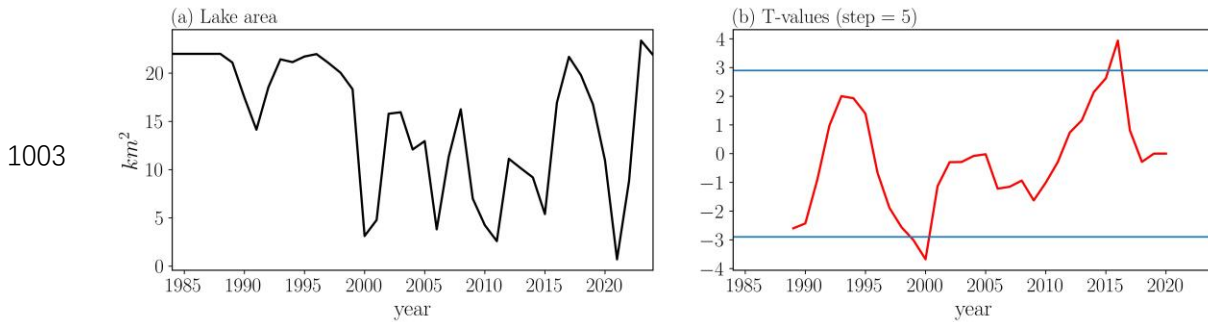
(a) Interannual variations of potential evapotranspiration; (b) multi-year mean seasonal variations of potential evapotranspiration; (c) interannual variations of the AI; (d) multi-year mean seasonal variations of the AI. Regional Drought Index

3.3.2 Impacts of hydro-climate elements on lake area

(1) Linear relationships between lake area and climatic variables

A sliding T-test on the lake area (Figure 16) reveals two turning points in the lake's area change, specifically in 2000 and 2015. Therefore, we divide the study period into

1000 three time segments: the first period from January 1984 to December 1999, the second
1001 period from January 2000 to December 2014, and the third period from January 2015
1002 to July 2024, to investigate the causes of the changes in lake area.



1004 **Figure 22-16 Time series and sliding T-test of the area of the Bahannao Lake Sliding T-test**

1005 The seasonal correlation analysis reveals pronounced differences in lake – climate
1006 relationships across seasons (Figure 17(a)). In spring, lake area exhibits a significant
1007 positive correlation with relative humidity (RH) ($r = 0.403$, $p < 0.01$) and a significant
1008 negative correlation with temperature (T) ($r = -0.352$, $p < 0.05$), indicating that spring
1009 lake-area variability is sensitive to atmospheric moisture conditions and warming
1010 processes. In contrast, correlations with precipitation (P) and potential
1011 evapotranspiration (PET) are weak and not statistically significant.

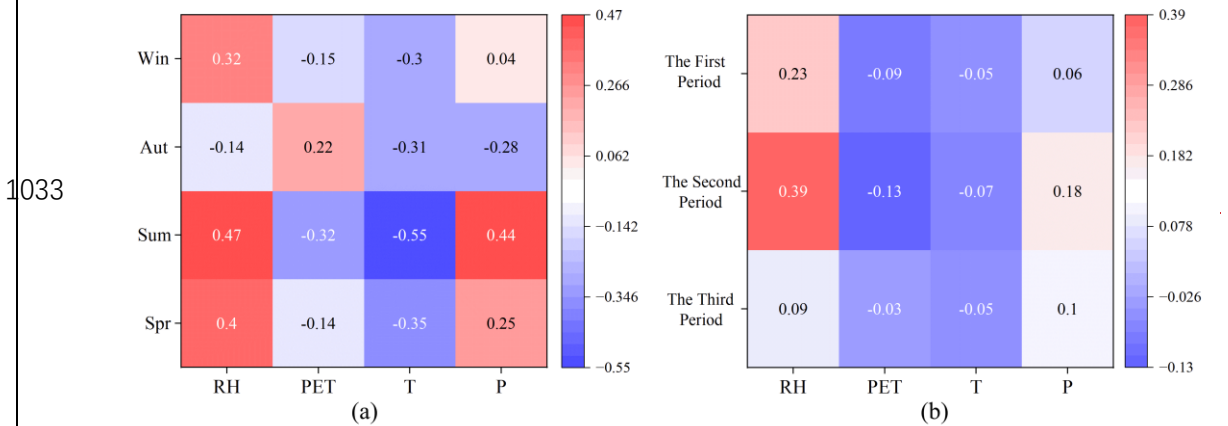
1012 During summer, the lake–climate relationships are strongest. Lake area shows
1013 significant negative correlations with temperature ($r = -0.549$, $p < 0.01$) and PET ($r =$
1014 -0.315 , $p < 0.05$), and significant positive correlations with precipitation ($r = 0.437$, p
1015 < 0.01) and RH ($r = 0.468$, $p < 0.01$). These results indicate that summer lake-area
1016 variability is jointly controlled by moisture supply and enhanced evaporative demand.

1017 In autumn, lake area is significantly negatively correlated only with temperature
1018 ($r = -0.315$, $p < 0.05$), whereas correlations with precipitation, RH, and PET are not

1019 significant, suggesting that autumn lake-area variations may reflect cumulative effects
 1020 of antecedent hydro-climatic conditions. In winter, lake area shows a significant
 1021 positive correlation with RH ($r = 0.315$, $p < 0.05$), while correlations with other climatic
 1022 variables remain weak, reflecting reduced hydrological activity during the cold season.

1023 At the interdecadal scale, lake - climate correlations exhibit clear stage-dependent
 1024 characteristics (Figure 17(b)). During the period 1984 - 1999, lake area shows no
 1025 significant correlation with temperature, precipitation, PET, or RH, indicating a
 1026 relatively weak response to individual climatic factors.

1027 During 2000 - 2014, lake area becomes significantly positively correlated with
 1028 precipitation ($p < 0.05$) and RH ($p < 0.01$), suggesting an enhanced sensitivity of lake-
 1029 area variability to moisture conditions during this period. In the most recent period
 1030 (2015 - 2024), lake area maintains a significant positive correlation only with RH ($p <$
 1031 0.05), while correlations with other climatic variables weaken, implying a dominant
 1032 role of atmospheric moisture conditions in regulating recent lake-area changes.



1034 Figure 17 Seasonal and interdecadal differences in correlations between lake area and climatic
 1035 drivers. (a) Seasonal correlations between lake area and RH, PET, T, and P. (b) Correlations between

lake area and climatic variables across three sub-periods (1984 - 1999, 2000 - 2014, and 2015 - 2024).

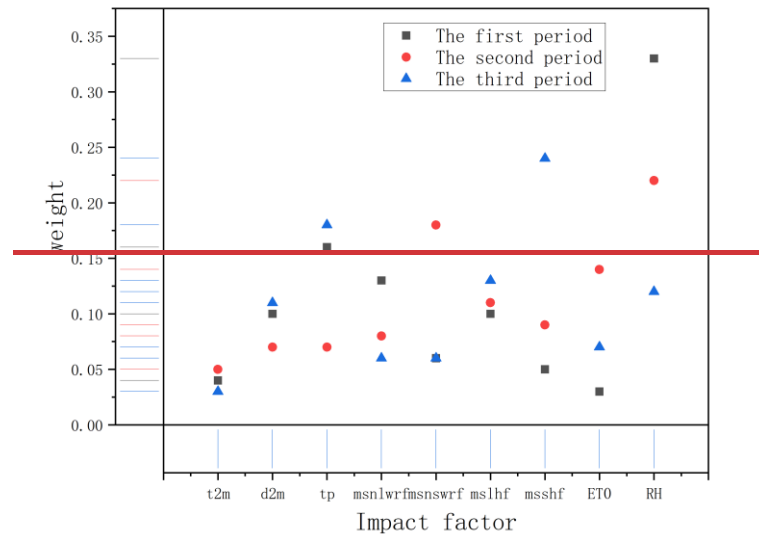


Figure 23 Factor Weight Diagram (Three Time Periods)

This paper conducts a factor analysis for three time periods, as shown in the figure 23. To better understand the causes of the change in the Bahai Nao lake area, we can explore several aspects in detail, including the direct and indirect effects of climate change, the roles of precipitation and evaporation, the effects of radiation and energy exchanges, and the combined effects of humidity and drought.

From 1984 to 1999, the change in Bahai Nao lake area was mainly driven by a decrease in precipitation and a decline in humidity. During this period, the main factors affecting lake area were humidity and precipitation. The weight of humidity reached 0.33, and that of precipitation was 0.16. This suggests that during this period, the decline in humidity significantly increased evaporation, leading to a reduction in lake area. Precipitation also decreased at a rate of 1.7355 mm per year, further exacerbating

1052 ~~the loss of lake water. Although temperature rose (at a rate of 0.0429°C per year), its~~
1053 ~~impact on lake area was relatively small (weight of 0.04).~~

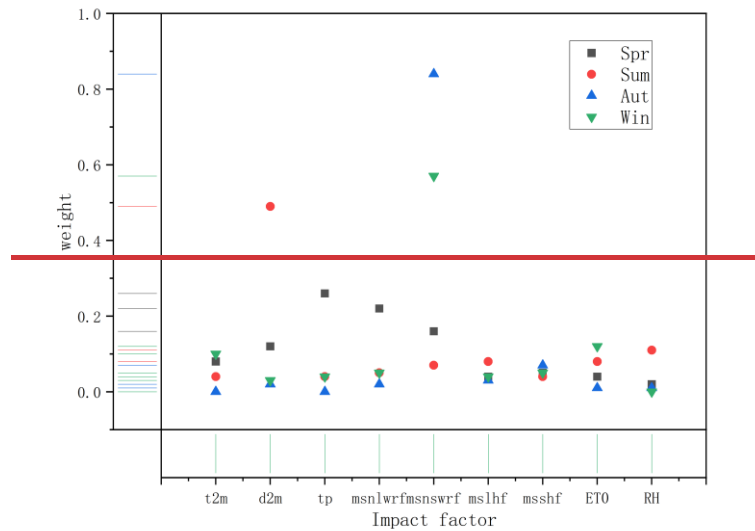
1054 ~~From January 2000 to December 2014, the main influencing factors were humidity~~
1055 ~~(weight of 0.22) and surface net longwave radiation (weight of 0.18). The decline in~~
1056 ~~humidity intensified evaporation, and the increase in surface net shortwave radiation~~
1057 ~~(at a rate of 0.0653 W/m² per year) also significantly influenced evaporation (weight of~~
1058 ~~0.08). The continuous decrease in precipitation (weight of 0.07) and changes in latent~~
1059 ~~heat flux (weight of 0.09) gradually reduced their impact on lake area.~~

1060 ~~From January 2015 to July 2024, the impact of sensible heat flux significantly~~
1061 ~~increased (weight of 0.24), reflecting an increased effect of surface heat exchange on~~
1062 ~~water evaporation. Meanwhile, the increase in potential evapotranspiration (weight of~~
1063 ~~0.13, with a rate of 1.9369 mm per year) indicated a sustained rise in water loss in the~~
1064 ~~region. Although temperature continued to rise (at a rate of 0.0429°C per year), its direct~~
1065 ~~impact on lake area was relatively limited (weight of 0.03). Additionally, the ongoing~~
1066 ~~decrease in precipitation (at a rate of 1.7355 mm per year) continued to contribute to~~
1067 ~~the shrinking of the lake area, and the decline in humidity (at a rate of 0.0987) further~~
1068 ~~exacerbated evaporation (weight of 0.07).~~

1069 ~~The driving factors of the Bahai Nao lake area changes show significant~~
1070 ~~differences in different time periods. From 1984 to 1999, humidity and precipitation~~
1071 ~~were the primary factors determining lake area change. Over time, from 2000 to 2014,~~
1072 ~~the impact of declining humidity and increasing shortwave radiation gradually~~
1073 ~~strengthened, while the effects of reduced precipitation and changes in latent heat flux~~

1074 weakened. From 2015 to 2024, the rise in temperature, increase in sensible heat flux,
1075 and the increase in potential evapotranspiration became the major drivers, making the
1076 trend of lake area shrinkage more significant.

1077 Overall, the reduction in the Bahai Nao lake area is primarily driven by the
1078 combined effects of climate warming, enhanced evaporation, and reduced precipitation.
1079 Particularly under the changes in humidity and evapotranspiration, the evaporation rate
1080 of the lake has notably accelerated.



1081

1082 **Figure 24 Weight of Influencing Factors by Season**

1083

1083 (2) Nonlinear hydro-climatic controls revealed by XGBoost

1084

1084 To further quantify the relative importance of climatic variables and explore
1085 potential nonlinear effects beyond linear correlations, an XGBoost model was applied
1086 using precipitation, temperature, relative humidity, and potential evapotranspiration as
1087 predictors.

1087

1088 Model evaluation indicates that training performance generally exceeds testing
1089 performance, and testing R^2 values are relatively low or even negative in some cases.

1089

1090 This behavior reflects the limited sample size, strong interannual variability, and
1091 inherent nonlinearity of lake-area dynamics in arid regions, rather than model
1092 inadequacy. Therefore, in this study, XGBoost is primarily used as an interpretative tool
1093 to assess the relative importance of climatic drivers rather than as a predictive model.

1094 XGBoost-derived feature importance exhibits clear seasonal contrasts that broadly
1095 agree with the correlation analysis while providing additional insights into nonlinear
1096 controls (Figure 18(a)). In spring, XGBoost feature importance indicates that air
1097 temperature is the most influential predictor (T, 0.31), followed by relative humidity
1098 (RH, 0.28), whereas precipitation (P, 0.20) and potential evapotranspiration (PET, 0.20)
1099 play secondary roles. This finding is consistent with the correlation analysis, which
1100 shows a significant positive correlation between lake area and RH ($r = 0.403$, $p < 0.01$)
1101 and a significant negative correlation with air temperature ($r = -0.352$, $p < 0.05$).
1102 Together, these results highlight the sensitivity of springtime lake dynamics to
1103 atmospheric moisture conditions and evaporative demand. Long-term trend analysis
1104 further indicates a significant increase in air temperature at a rate of $0.043\text{ }^{\circ}\text{C yr}^{-1}$ ($p <$
1105 0.001) and a significant decline in RH (-0.099 yr^{-1} , $p = 0.009$), reinforcing the role of
1106 enhanced evaporation and atmospheric drying in shaping spring lake-area changes.

1107 In summer, air temperature (T, 0.35) and relative humidity (RH, 0.26) dominate
1108 the feature-importance rankings, with precipitation (P, 0.18) and potential
1109 evapotranspiration (PET, 0.21) also contributing substantially. This aligns well with the
1110 correlation results, which indicate that summer lake area is positively correlated with
1111 precipitation ($r = 0.437$, $p < 0.01$) and RH ($r = 0.468$, $p < 0.01$), and negatively

1112 correlated with temperature ($r = -0.549$, $p < 0.01$) and PET ($r = -0.315$, $p < 0.05$). Trend
1113 analysis shows that although precipitation exhibits a decreasing tendency (-1.736 mm
1114 yr^{-1} , $p = 0.135$, not significant), PET increases significantly at a rate of 1.937 mm yr^{-1}
1115 ($p = 0.01$). This suggests that summer lake-area variability is increasingly constrained
1116 by enhanced evaporative demand, with the balance between water input and
1117 evaporation losses playing a dominant role.

1118 In autumn, linear correlations between lake area and most climatic variables are
1119 weak and statistically insignificant. However, XGBoost results still indicate relatively
1120 high importance for relative humidity (RH, 0.34) and potential evapotranspiration (PET,
1121 0.31), suggesting that autumn lake dynamics may be governed by nonlinear processes
1122 or threshold effects that are not adequately captured by linear methods alone.
1123 Considering the significant upward trend in PET and the declining tendency of the
1124 aridity index (AI; -0.015 yr^{-1} , $p = 0.07$), autumn lake systems appear to be transitioning
1125 toward evaporation-dominated control.

1126 In winter, overall feature importance values are relatively low due to reduced
1127 hydrological activity, yet relative humidity (RH, 0.34) remains the most influential
1128 variable in the XGBoost model. This is consistent with the correlation analysis showing
1129 a significant positive relationship between winter lake area and RH ($r = 0.315$, $p < 0.05$),
1130 indicating that background atmospheric moisture conditions still serve as an important
1131 indicator of lake variability during the frozen period. Subsequently, a seasonal analysis
1132 of the influencing factors on the lake area of Bahai Nao Lake in spring, summer, autumn,
1133 and winter was conducted, as shown in Figure 24.

1134
1135
1136
1137
1138
1139
1140
1141
1142
1143
1144
1145
1146
1147
1148
1149
1150
1151
1152
1153
1154
1155

At the decadal scale, XGBoost results reveal a clear temporal shift in the dominant climatic controls on lake-area variability, as shown in figure 18(b). During 1984 - 1999, the importance of individual climatic variables is generally low and dispersed, consistent with the weak correlations observed during this period. This suggests that the lake system exhibited relatively low sensitivity to climatic fluctuations in the early stage.

During 2000 - 2014, precipitation (P, 0.22), potential evapotranspiration (PET, 0.23) and relative humidity (RH, 0.34) show markedly higher importance in the XGBoost model, in agreement with correlation results indicating significant positive relationships between lake area and precipitation ($r = 0.179$, $p < 0.05$) and RH ($r = 0.388$, $p < 0.01$). This period is therefore characterized by a precipitation- and moisture-dominated control regime.

In the most recent period (2015 - 2024), the importance of temperature and PET increases noticeably, while the contribution of precipitation weakens. Combined with the observed warming trend and enhanced evaporative demand, these results indicate a transition toward an evaporation-dominated climatic control on lake-area dynamics in recent years.~~From the previous analysis, the climate conditions in spring were: temperature 10.16°C, 2-meter dew point temperature 6.28°C, rainfall 76.14 mm, average net long-wave radiation 103.13 W/m², potential evapotranspiration 456.37 mm, and humidity 36.62%.~~

1156 By integrating long-term trend analysis, linear correlation analysis, and XGBoost-
1157 based nonlinear feature importance, this study demonstrates that lake-area variability
1158 in arid regions is not governed by a single climatic factor, but rather by the interplay
1159 between water supply and evaporative demand across different seasons and time scales.
1160 Linear correlation analysis effectively captures the summer lake - climate relationship
1161 dominated by water balance, whereas the nonlinear XGBoost approach provides
1162 complementary insights into more complex control mechanisms during transitional
1163 seasons such as spring and autumn. Overall, the results indicate that with continued
1164 regional warming, increasing PET, and intensifying aridity, evaporative processes are
1165 playing an increasingly important role in controlling lake-area variability, offering
1166 important implications for understanding the response of arid-region lakes to future
1167 climate change.~~Spring is the main replenishment period for rainfall, with a weight of~~
1168 ~~0.26, significantly higher than the other seasons. Therefore, although the 76.14 mm of~~
1169 ~~rainfall is not as abundant as in summer, it still plays an important role in replenishing~~
1170 ~~the lake's water volume. At the same time, radiation energy (103.13 W/m²) and~~
1171 ~~relatively low humidity lead to significant evaporation. The high potential~~
1172 ~~evapotranspiration of 456.37 mm also indicates that the evaporation potential in spring~~
1173 ~~is high, which could partly offset the water replenishment brought by the rainfall. This~~
1174 ~~is why the increase in lake water volume is slow in spring.~~

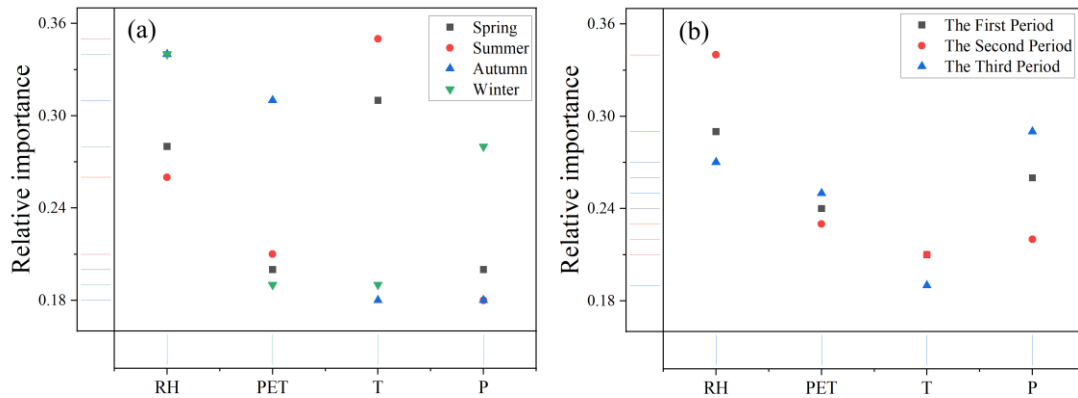


Figure 18 Weight of influencing factors by season

Abbreviations: RH denotes relative humidity (%); PET denotes potential evapotranspiration (mm);

T denotes air temperature (°C); P denotes precipitation (mm). In summer, the climate conditions

were: temperature 21.58°C, 2-meter dew point temperature 11.06°C, rainfall 229.87 mm, average

net long-wave radiation 89.14 W/m², potential evapotranspiration 620.36 mm, and humidity

53.58%.

Summer is the season with the most abundant rainfall (229.87 mm), which is a key replenishment

period for the lake's water volume. However, the high weight of the 2-meter dew point temperature

(0.49) indicates that humidity controls the evaporation of the water body. Due to the high humidity

(53.58%), the evaporation rate of the lake is relatively low. Despite the very high potential

evapotranspiration (620.36 mm), the impact of humidity significantly slows down the evaporation

of moisture, allowing the lake area to maintain relatively well during the summer.

In autumn, the climate conditions were: temperature 7.86°C, 2-meter dew point temperature 0.78°C,

rainfall 96.58 mm, average net long-wave radiation 83.52 W/m², average net short-wave radiation

124.12 W/m², potential evapotranspiration 314.29 mm, and humidity 55.91%.

The variation in lake water volume in autumn is mainly driven by solar short-wave radiation, with

a weight of 0.84. This indicates that although the rainfall in autumn is moderate (96.58 mm), the

1194 higher short wave radiation (124.12 W/m^2) leads to intense evaporation. The potential
1195 evapotranspiration is 314.29 mm , showing that the lake evaporation is large, and although the
1196 relative humidity is relatively high (55.91%), it is insufficient to prevent the reduction of the lake
1197 water volume. The low temperature in autumn (7.86°C) further indicates that although the
1198 temperature impact is minimal, the radiation intensity still determines the seasonal reduction in lake
1199 area.

1200 in winter, the climate conditions were: temperature 2.79°C , 2-meter dew point temperature 14.66°C ,
1201 rainfall 26.54 mm , average net long wave radiation 88.52 W/m^2 , average net short wave radiation
1202 114.66 W/m^2 , potential evapotranspiration 200.32 mm , and humidity 44.03% .

1203 Winter sees a significant decrease in temperature (2.79°C), and evaporation is suppressed. However,
1204 the surface short wave radiation remains the main influencing factor in winter, with a weight of 0.57 .
1205 This suggests that, despite the lower rainfall (26.54 mm) in winter, radiation still plays a role in
1206 moisture evaporation. The potential evapotranspiration is 200.32 mm , which is lower compared to
1207 other seasons, but still enough to affect the lake's water volume. The temperature has a small
1208 contribution to the lake water volume change (0.10), indicating that in winter, the main evaporation
1209 driving force is solar radiation.

1210 In summary, the seasonal variation of Bahai Nao Lake's water volume is mainly affected by rainfall,
1211 radiation, humidity, and evapotranspiration. In spring, the change in lake area is primarily
1212 determined by rainfall replenishment, but higher radiation and potential evapotranspiration weaken
1213 the accumulation of water. In summer, humidity and dew point temperature are the dominant factors
1214 affecting the lake area. Despite abundant rainfall, high humidity slows down evaporation,
1215 maintaining the lake's water volume. In autumn, due to intense solar short wave radiation, the lake

1216 ~~water volume decreases significantly, with evaporation being the dominant factor. In winter, despite~~
1217 ~~the low temperature, radiation remains the main driving factor for evaporation, leading to a~~
1218 ~~continued reduction in the lake's water volume.~~

1219 ~~This seasonal hydrological change in the lake suggests that different seasonal factors influencing~~
1220 ~~the lake area focus on the interaction between rainfall and radiation, as well as the regulatory effect~~
1221 ~~of humidity on evaporation.~~

1222 **4. Discussion**

1223 This study constructed a continuous monthly lake-area time series for Bahannao
1224 Lake spanning 1984 - 2024 using an optimized lake-area extraction framework that
1225 integrates seasonal water-index selection, adaptive thresholding, maximum
1226 connectivity analysis, and mutual information - based gap filling. Compared with
1227 widely used long-term products such as the JRC Global Surface Water dataset, which
1228 are often constrained by cloud contamination, seasonal ice cover, and temporal
1229 discontinuities, the proposed framework substantially improves temporal continuity
1230 and robustness under complex environmental conditions. This improvement is
1231 particularly important for small lakes in arid and semi-arid regions, where data gaps
1232 and seasonal disturbances are pervasive in existing datasets.

1233 At the methodological level, this study introduces targeted improvements at
1234 several critical steps relative to previous approaches. First, the seasonal application of
1235 NDWI and MNDSI for non-freezing and freezing periods, respectively, enhances the
1236 stability of water-body identification under varying surface conditions, outperforming
1237 traditional single-index methods (McFeeters, 1996; Yao et al., 2015). Second, the

1238 combination of Otsu thresholding with DEM-based terrain constraints effectively
1239 reduces misclassification caused by topographic shadows and complex terrain, which
1240 is a common challenge for inland lakes in arid environments. Third, the mutual
1241 information - based image-filling strategy reconstructs cloud- and stripe-contaminated
1242 pixels by matching historically most similar cloud-free images, thereby extending the
1243 usability of long-term Landsat archives. Compared with approaches relying solely on
1244 interpolation (Zhao and Gao, 2018), this strategy substantially improves the
1245 completeness and reliability of multi-decadal lake-area records. Collectively, these
1246 methodological enhancements systematically address key challenges repeatedly
1247 identified in previous studies, including cloud contamination, seasonal variability,
1248 topographic interference, and spectral complexity of inland waters (Mouw et al., 2015;
1249 Palmer et al., 2015; Shen et al., 2017; Cao et al., 2019), and establish a transferable
1250 framework suitable for lake monitoring in arid and data-scarce regions.

1251 From a hydro-climatic perspective, the reconstructed long-term record provides
1252 important insights into the mechanisms controlling lake dynamics in arid environments.
1253 Consistent with previous studies, precipitation and evaporation emerge as the primary
1254 factors regulating lake-area variability, particularly during the warm season when both
1255 water inputs and evaporative losses are enhanced (Tao et al., 2015; Li et al., 2017). The
1256 correlation analysis indicates that lake area is significantly positively correlated with
1257 precipitation and relative humidity in summer, whereas atmospheric moisture
1258 conditions exert a more pronounced influence during spring and winter. These findings
1259 reinforce the view that lake dynamics in arid regions are governed by the seasonal

1260 balance between water supply and evaporative demand.

1261 However, compared with many existing studies that rely primarily on annual-scale
1262 analyses, the monthly lake-area time series developed here reveals pronounced seasonal
1263 heterogeneity and transitional behavior. In spring and autumn, linear correlations
1264 between lake area and individual climatic variables are generally weak, whereas
1265 XGBoost feature-importance analysis consistently identifies relative humidity and
1266 potential evapotranspiration as influential factors. This discrepancy suggests that lake
1267 responses during transitional seasons may be governed by nonlinear processes or
1268 threshold effects that cannot be fully captured by linear statistical methods alone. The
1269 combined use of correlation analysis and XGBoost therefore provides complementary
1270 perspectives on lake – climate relationships across different temporal scales.

1271 At the decadal scale, both correlation analysis and XGBoost results indicate a clear
1272 evolution in dominant climatic controls on lake-area variability. During 2000 – 2014,
1273 precipitation and relative humidity exhibit increased importance and significant
1274 positive associations with lake area, indicating a moisture-dominated control regime.
1275 In contrast, during 2015 – 2024, the importance of air temperature and potential
1276 evapotranspiration increases markedly, while the contribution of precipitation weakens.
1277 This shift reflects a transition toward evaporation-dominated control under sustained
1278 warming conditions and highlights a dynamic reorganization of hydro-climatic drivers.
1279 Such temporal evolution extends existing understanding by explicitly demonstrating
1280 how dominant controls on arid-region lakes can shift under intensified climate
1281 variability.

1282 These results have broader implications for studies of lakes in arid and semi-arid
1283 regions. The fragile water balance and limited buffering capacity of dryland lakes
1284 render them highly sensitive to even modest changes in precipitation, atmospheric
1285 moisture, and evaporative demand. The observed transition from precipitation-
1286 dominated to evaporation-dominated control suggests increasing vulnerability of arid-
1287 region lakes under ongoing climate warming. Even in the absence of a pronounced
1288 decline in precipitation, enhanced evaporation and atmospheric drying may offset or
1289 exceed water inputs, thereby accelerating lake shrinkage. This finding underscores the
1290 necessity of considering multiple hydro-climatic factors simultaneously when assessing
1291 future lake trajectories in arid environments.

1292 From a water-resources management perspective, the results indicate that lake
1293 conservation and management strategies in arid regions should not focus solely on
1294 precipitation trends but must also account for changes in evaporative demand, drought
1295 intensity, and atmospheric moisture conditions. The lake-area extraction framework and
1296 the insights into evolving climatic controls presented here provide a robust technical
1297 foundation for long-term lake monitoring, risk assessment, and adaptive water-
1298 management strategies in data-sparse dryland regions.

1299 Several limitations of this study should be acknowledged. First, while remote
1300 sensing reliably captures surface-area dynamics, subsurface processes such as
1301 groundwater inflow and outflow were not explicitly quantified and may influence lake
1302 water balance. Second, the 30 m spatial resolution of Landsat data limits detection of
1303 fine-scale shoreline changes, and future studies could benefit from integrating higher-

1304 resolution sensors such as Sentinel-2. Third, although XGBoost effectively captures
1305 nonlinear relationships, its data-driven nature limits physical interpretability relative to
1306 process-based hydrological models. Future research could integrate remote sensing,
1307 machine learning, ecohydrological modeling, and socioeconomic data to further
1308 advance understanding of lake dynamics in arid regions.

1309 This study established a continuous monthly record of Bahannao Lake from 1984
1310 to 2024 using an optimized extraction framework that integrates seasonal index
1311 selection, maximum connectivity analysis, and mutual information-based gap filling.
1312 Unlike previous long-term products such as the JRC Global Surface Water dataset,
1313 which are often constrained by cloud contamination and temporal discontinuity, our
1314 framework ensures both higher temporal continuity and robustness under complex
1315 environmental conditions.

1316 The methodological improvements provide several advantages. First, the seasonal
1317 use of NDWI and MNDSI effectively distinguishes water bodies under freezing and
1318 non-freezing conditions, outperforming traditional single-index approaches (McFeeters,
1319 1996; Yao et al., 2015). Second, the combination of Otsu thresholding with DEM
1320 constraints reduces misclassification from shadows and topography, a common issue in
1321 arid-region lakes with irregular terrain. Third, the MI-based filling strategy reconstructs
1322 cloud and stripe-contaminated images, extending the applicability of Landsat data and
1323 providing a longer, more reliable time series compared with interpolation-only methods
1324 (Zhao and Gao, 2018). Together, these innovations establish a transferable framework
1325 for dynamic lake monitoring, particularly suited for arid and data-scarce regions where

1326 ~~conventional products often fail. Importantly, these improvements systematically~~
1327 ~~address the common challenges highlighted in earlier studies, including cloud~~
1328 ~~contamination, seasonal variations, topographic interference, and spectral complexity~~
1329 ~~in inland waters (Mouw et al., 2015; Palmer et al., 2015; Shen et al., 2017; Cao et al.,~~
1330 ~~2019).~~

1331 ~~Beyond methodological advances, the long-term record reveals important insights~~
1332 ~~into the hydro-climatic controls of arid-region lakes. Precipitation was identified as the~~
1333 ~~dominant driver of lake expansion in spring and summer, while shortwave radiation~~
1334 ~~governed evaporation in autumn and winter. This seasonal contrast aligns with findings~~
1335 ~~from other arid and high-altitude regions, such as Nam Co on the Tibetan Plateau (Li et~~
1336 ~~al., 2017) and lakes on the Mongolian Plateau (Tao et al., 2015), where radiation and~~
1337 ~~humidity strongly modulate evaporation under limited precipitation inputs. However,~~
1338 ~~our results also highlight a pronounced nonlinear shift in dominant drivers over time:~~
1339 ~~humidity and precipitation before 2000, radiation and humidity variability during~~
1340 ~~2000–2014, and energy flux intensification after 2015. This temporal evolution differs~~
1341 ~~from some humid-region lakes, where nutrient enrichment or human disturbance~~
1342 ~~dominate changes (Jeppesen et al., 2014), suggesting that climatic forcing plays a more~~
1343 ~~persistent role in arid environments.~~

1344 ~~These findings carry broader implications for ecohydrological research and water~~
1345 ~~resource management. By quantifying the nonlinear interactions of multiple climatic~~
1346 ~~factors, our study demonstrates that lake dynamics in arid regions cannot be attributed~~
1347 ~~to a single driver but emerge from the shifting balance of precipitation, radiation, and~~

1348 ~~evapotranspiration. This highlights the vulnerability of arid region lakes to climate~~
1349 ~~change, where even moderate increases in radiation or evapotranspiration can outweigh~~
1350 ~~precipitation recovery. Such insights are crucial for improving hydrological models,~~
1351 ~~projecting future lake dynamics, and informing adaptive management strategies under~~
1352 ~~intensified drought risk.~~

1353 ~~Several limitations should be acknowledged. First, while remote sensing provides~~
1354 ~~a robust record of surface area, subsurface processes such as groundwater inflow and~~
1355 ~~outflow were not explicitly considered, which may contribute to lake water balance.~~
1356 ~~Second, the spatial resolution of Landsat (30 m) limits the detection of small scale~~
1357 ~~shoreline changes, and higher resolution sensors (e.g., Sentinel 2) could improve~~
1358 ~~accuracy in future studies. Third, although XGBoost effectively captured nonlinear~~
1359 ~~relationships, its “black box” nature limits interpretability compared with process-~~
1360 ~~based hydrological models. Future research could combine machine learning with~~
1361 ~~ecohydrological modeling and socioeconomic datasets to better quantify the combined~~
1362 ~~impacts of climate variability and human activities on arid region lakes.~~

1363 **5. Conclusion**

1364 This study developed an optimized remote-sensing framework to construct a
1365 continuous monthly lake-area time series for Bahannao Lake from 1984 to 2024. By
1366 integrating seasonal water-index selection, adaptive thresholding, connectivity analysis,
1367 and mutual information-based image reconstruction, the proposed method effectively
1368 overcomes common limitations associated with cloud contamination, seasonal ice
1369 cover, and data gaps in long-term Landsat archives. Validation using Hongjiannao Lake

1370 and Wuliangsu Lake further demonstrates the robustness and regional applicability
1371 of the framework for lake monitoring in arid and semi-arid environments.

1372 The reconstructed time series reveals pronounced interannual variability and
1373 strong seasonal contrasts in lake-area dynamics. Linear correlation analysis indicates
1374 that lake-area variations are primarily associated with precipitation and atmospheric
1375 moisture conditions during the warm season, whereas evaporative demand plays an
1376 increasingly important role during cold and transitional seasons. The combined use of
1377 correlation analysis and XGBoost modeling further reveals a clear stage-dependent
1378 evolution of climatic controls. During 1984-1999, lake dynamics were mainly
1379 associated with humidity and precipitation variability; during 2000-2014, the influence
1380 of moisture-related conditions remained important under enhanced climate variability;
1381 and during 2015-2024, rising air temperature and potential evapotranspiration emerged
1382 as dominant contributors, indicating a transition toward evaporation-dominated control
1383 under sustained warming.

1384 Overall, the results demonstrate that lake-area changes in arid regions are
1385 governed by nonlinear and evolving interactions between water supply and evaporative
1386 demand rather than by any single climatic factor. By combining high-temporal-
1387 resolution lake-area reconstruction with both linear and nonlinear analytical approaches,
1388 this study provides new insights into the mechanisms underlying arid-region lake
1389 dynamics. The proposed framework offers a valuable tool for long-term lake
1390 monitoring and contributes to improved understanding of eco-hydrological responses
1391 and water-resource vulnerability under ongoing climate change in dryland

1392 ~~regions. study developed an optimized lake area extraction framework and applied it to~~
1393 ~~construct a continuous monthly record of Bahannao Lake from 1984 to 2024. The~~
1394 ~~method integrates seasonal index selection, adaptive thresholding, maximum~~
1395 ~~connectivity analysis, and mutual information based gap filling, effectively~~
1396 ~~addressing cloud contamination, seasonal freezing, and data gaps in remote sensing~~
1397 ~~images.~~

1398
1399 ~~The long term record reveals both significant interannual variability and clear~~
1400 ~~seasonal differences in lake dynamics. Precipitation was the dominant driver of~~
1401 ~~lake expansion in spring and summer, whereas shortwave radiation controlled~~
1402 ~~evaporation in autumn and winter. Factor weights further demonstrate a~~
1403 ~~temporal shift in dominant mechanisms: humidity decline and precipitation~~
1404 ~~reduction before 2000; enhanced radiation and humidity variability during~~
1405 ~~2000–2014; and intensified sensible heat flux and potential evapotranspiration~~
1406 ~~after 2015.~~

1407 ~~These findings highlight the nonlinear and evolving interactions of hydro~~
1408 ~~climatic drivers regulating arid region lakes. The proposed framework not only~~
1409 ~~improves the reliability of long term lake monitoring but also provides~~
1410 ~~actionable insights for ecohydrological research, water resource management,~~
1411 ~~and climate change adaptation in arid environments.~~

1412 **Competing interests**

1413 The authors declare that they have no conflict of interest.

1414 **Code/Data availability**

1415 The data and code that support the findings of this study are available from the
1416 corresponding author upon reasonable request.

1417 **Author contribution**

1418 R Z and X W conceived and designed the study, developed the methodology,
1419 curated the data, and performed the formal analysis. R Z was responsible for
1420 visualization. R Z and X W prepared the original draft of the manuscript, and all authors
1421 contributed to reviewing and editing the paper. X W provided overall supervision.

1422 **Acknowledgments**

1423 We are grateful to the National Key R&D Program of China (No.
1424 2023YFC3206504), National Natural Science Foundation of China (No. 52121006,
1425 41961124006), Postgraduate Thesis Fund of Nanjing Hydraulic Research
1426 Institute(Yy524010), Young Top-Notch Talent Support Program of National High-level
1427 Talents Special Support Plan, and Research Project of Ministry of Natural Resources
1428 (No. 20210103), Research Project of Academy of Science and Technology of Inner
1429 Mongolia (No. 2024RCYJ05003) for providing financial support for this research. We
1430 are also thankful international key authors and their agencies. We are also thankful to
1431 anonymous reviewers and editors for their helpful comments and suggestions.

1432 **References**

1433 [Adrian R, O'Reilly C M, Zagarese H, et al. Lakes as sentinels of climate change \[J\].](#)

1434 [Limnology and Oceanography, 2009, 54\(6part2\): 2283-2297](#)

1435 [Bergé-Nguyen M, Crétaux J F. Inundations in the Inner Niger Delta: Monitoring and](#)

1436 [analysis using MODIS and global precipitation datasets \[J\]. Remote Sensing, 2015,](#)
1437 [7\(2\): 2127-2151.](#)

1438 [Busker T, de Roo A, Gelati E, et al. A global lake and reservoir volume analysis using](#)
1439 [a surface water dataset and satellite altimetry\[J\]. Hydrology and Earth System](#)
1440 [Sciences, 2019, 23\(2\): 669-690.](#)

1441 [Cao Z G, Ma R H, Duan H T, et al. A machine learning approach to estimate](#)
1442 [chlorophyll-a from Landsat-8 measurements in inland lakes \[J\]. Remote Sensing](#)
1443 [of Environment, 2020, 248: 111974](#)

1444 [Cao Z G, Ma R H, Duan H T, et al.. Effects of broad bandwidth on the remote sensing](#)
1445 [of inland waters: implications for high spatial resolution satellite data applications](#)
1446 [\[J\]. ISPRS Journal of Photogrammetry and Remote Sensing, 2019, 153: 110-122](#)

1447 [Carroll M L, Townshend J R G, DiMiceli C M, et al. Shrinking lakes of the Arctic:](#)
1448 [Spatial relationships and trajectory of change\[J\]. Geophysical Research Letters,](#)
1449 [2011, 38\(20\).](#)

1450 [Cooley S W, Smith L C, Stepan L, et al. Tracking dynamic northern surface water](#)
1451 [changes with high-frequency planet CubeSat imagery\[J\]. Remote Sensing, 2017,](#)
1452 [9\(12\): 1306.](#)

1453 [Donchyts G, Baart F, Winsemius H, et al. Earth's surface water change over the past 30](#)
1454 [years\[J\]. Nature Climate Change, 2016, 6\(9\): 810-813.](#)

1455 [Grant L, Vanderkelen I, Gudmundsson L, et al. Attribution of global lake systems change](#)
1456 [to anthropogenic forcing\[J\]. Nature Geoscience, 2021, 14\(11\):849-854.](#)

1457 [Guan L G. Morphological evolution and ecological function positioning of Ulansuhai](#)

1458 Lake under the influence of human activities[J]. Inner Mongolia Water Resources,
1459 2022, (08): 8 - 10.

1460 Huang C, Chen Y, Zhang S, et al. Detecting, extracting, and monitoring surface water
1461 from space using optical sensors: A review[J]. Reviews of Geophysics, 2018, 56(2):
1462 333-360.

1463 Jeppesen E, Meerhoff M, Davidson T, et al. Climate change impacts on lakes: an
1464 integrated ecological perspective based on a multi-faceted approach, with special
1465 focus on shallow lakes[J]. Journal of Limnology, 2014, 73.

1466 Ji L W, Wang Z W, Cui L L, et al. Remote sensing monitoring of spatiotemporal
1467 dynamics of Hongjiannao Lake over the past 30 years[J]. Shaanxi Meteorology,
1468 2023(1): 41 - 49.

1469 Klein I, Gessner U, Dietz A J, et al. Global WaterPack - A 250 m resolution dataset
1470 revealing the daily dynamics of global inland water bodies[J]. Remote sensing of
1471 environment, 2017, 198: 345-362.

1472 Kravitz J, Matthews M, Lain L, et al. Potential for high fidelity global mapping of
1473 common inland water quality products at high spatial and temporal resolutions
1474 based on a synthetic data and machine learning approach[J]. Frontiers in
1475 Environmental Science, 2021, 9: 58766

1476 LABA Zhuoma, DEJI Yangzong, LA Ba, et al. Remote sensing analysis on the area
1477 variations of Tangra Yutso in Tibetan Plateau over the past 40 years [J]. Lake
1478 Science,2017,29(02):480-489.

1479 Li M, Yan D H, Liu S H, et al, Variation Characteristics of Water Surface Area and

1480 Water Storage Capacity of Namucuo Lake in Recent 40 Years [J].Water Resources
1481 and Power, 2017, 35 (02): 41-43+52.

1482 Li S, Qu W, Zhang T T, et al. Study on changes in water surface area and water volume
1483 of Ulansuhai Lake based on remote sensing imagery[J]. Yellow River, 2023,
1484 45(S1): 22 - 23.

1485 Li, L., Long, D., Wang, Y. et al. Global dominance of seasonality in shaping lake-
1486 surface-extent dynamics. Nature (2025). [https://doi.org/10.1038/s41586-025-](https://doi.org/10.1038/s41586-025-09046-3)
1487 09046-3

1488 Liu Y B, Wu G P, Zhao X S, et al. Remote sensing for watershed hydrology: issues and
1489 challenges [J]. Advances in Earth Science, 2020, 35(5): 488-496

1490 Liu Y , Yue H. Analysis of Hongjiannao Lake Area Based on SMMI[J]. Science
1491 Technology and Engineering, 2016, 16(16): 122-127.

1492 Liu Z W, Su Y L and Yang L. Limnology is a multidisciplinary and integrative science
1493 for studying inland waters: with special reference to the challenges and
1494 opportunities for the development of limnology in China [J]. Journal of Lake
1495 Sciences, 2020, 32(5): 1244-1253

1496 Ma H L, Bai M, Guo Y. Analysis on the Space—time Evolvement Process and Cause
1497 of Hongjiannao during 1957 and 2019[J]. Geomatics & Spatial Information
1498 technology, 2020, 43(12): 143-146.

1499 Ma R H, Duan H T, Hu C M, et al. half-century of changes in China’s lakes: global
1500 warming or human influence? [J]. Geophysical Research Letters, 2010, 37(24):
1501 L24106

1502 [Ma R H, Yang G S, Duan H T, et al. China's lakes at present: number, area and spatial](#)
1503 [distribution \[J\]. Science China Earth Sciences, 2011, 54\(2\): 283-289](#)

1504 [Ma Y, Xu N, Zhang W H, et al. Increasing water levels of global lakes between 2003](#)
1505 [and 2009 \[J\]. IEEE Geoscience and Remote Sensing Letters, 2020b, 17\(2\): 187-](#)
1506 [191](#)

1507 [McFeeters S K. The use of the Normalized Difference Water Index \(NDWI\) in the](#)
1508 [delineation of open water features\[J\]. International journal of remote sensing, 1996,](#)
1509 [17\(7\): 1425-1432.](#)

1510 [Mouw C B, Greb S, Aurin D, et al. Aquatic color radiometry remote sensing of coastal](#)
1511 [and inland waters: challenges and recommendations for future satellite missions](#)
1512 [\[J\]. Remote Sensing of Environment, 2015, 160: 15-30](#)

1513 [Palmer S C J, Kutser T and Hunter P D. Remote sensing of inland waters: challenges,](#)
1514 [progress and future directions \[J\]. Remote Sensing of Environment, 2015, 157: 1-](#)
1515 [8](#)

1516 [Pekel J F, Cottam A, Gorelick N, et al. High-resolution mapping of global surface water](#)
1517 [and its long-term changes \[J\]. Nature, 2016, 540\(7633\): 418-422](#)

1518 [Pekel J F, Vancutsem C, Bastin L, et al. A near real-time water surface detection method](#)
1519 [based on HSV transformation of MODIS multi-spectral time series data\[J\].](#)
1520 [Remote sensing of environment, 2014, 140: 704-716.](#)

1521 [Pickens A H, Hansen M C, Hancher M, et al. Mapping and sampling to characterize](#)
1522 [global inland water dynamics from 1999 to 2018 with full Landsat time-series \[J\].](#)
1523 [Remote Sensing of Environment, 2020, 243: 111792](#)

1524 Plug L J, Walls C, Scott B M. Tundra lake changes from 1978 to 2001 on the
1525 Tuktoyaktuk Peninsula, western Canadian Arctic[J]. Geophysical Research
1526 Letters, 2008, 35(3).

1527 Preston D L, Caine N, McKnight D M, et al. Climate regulates alpine lake ice cover
1528 phenology and aquatic ecosystem structure[J]. Geophysical Research Letters,
1529 2016, 43(10): 5353-5360.

1530 Råman Vinnå L, Medhaug I, Schmid M, et al. The vulnerability of lakes to climate
1531 change along an altitudinal gradient[J]. Communications Earth & Environment,
1532 2021, 2(1): 35.

1533 Rossow W B, Schiffer R A. Advances in understanding clouds from ISCCP[J]. Bulletin
1534 of the American Meteorological Society, 1999, 80(11): 2261-2288.

1535 Schmid M, Hunziker S, Wüest A. Lake surface temperatures in a changing climate: a
1536 global sensitivity analysis[J]. Climatic change, 2014, 124:301-315.

1537 Secretariat G. Implementation plan for the global observing system for climate in
1538 support of the UNFCCC (2010 Update) [C]//Proceedings of the Conference of the
1539 Parties (COP), Copenhagen, Denmark. 2009: 7-18.

1540 Shen M, Duan H T, Cao Z G, et al. Determination of the downwelling diffuse
1541 attenuation coefficient of lake water with the Sentinel-3A OLCI [J]. Remote
1542 Sensing, 2017, 9(12): 1246

1543 Tan R J, Ma Q, Wang R. Remote sensing monitoring of long-term time-series dynamics
1544 of water area and aquatic vegetation, Yellow River 2021, 43(S2):77-79

1545 Tao S, Fang J, Zhao X, et al. Rapid loss of lakes on the Mongolian Plateau[J].

1546 [Proceedings of the National Academy of Sciences, 2015, 112\(7\): 2281-2286.](#)

1547 [Tong Y, Feng L, Wang X, et al. Global lakes are warming slower than surface air](#)

1548 [temperature due to accelerate devaporation \[J\]. Nature Water, 2023,1\(11\):929-940](#)

1549 [Vincent W F. Effects of climate change on lakes\[J\]. 2009.](#)

1550 [Wang J, Song C, Reager J T, et al. Recent global decline in endorheic basin water](#)

1551 [storages\[J\]. Nature geoscience, 2018, 11\(12\): 926-932.](#)

1552 [Wang Y, Yan Z L, Gao F. Monitoring spatio-temporal changes of water area in](#)

1553 [Hongjiannao Lake from 1957 to 2015 and its driving forces analysis\[J\].](#)

1554 [Transactions of the Chinese Society of Agricultural Engineering, 2018, 34\(02\):](#)

1555 [265-271.](#)

1556 [Woolway R I, Kraemer B M, Lenters J D, et al. Global lake responses to climate](#)

1557 [change\[J\]. Nature Reviews Earth & Environment, 2020, 1\(8\): 388-403.](#)

1558 [Xie Z G, Lian Y X, Wu H P, et al. Water Area Change of Hongjiannao Wetland from](#)

1559 [2000 to 2018 and Related Policies\[J\]. Shaanxi Forest Science and Technology,](#)

1560 [2021, 49\(4\): 33-38.](#)

1561 [Yang G S, Ma R H, Zhang L, et al. Lake status, major problems and protection strategy](#)

1562 [in China \[J\]. Journal of Lake Sciences, 2010, 22\(6\): 799-810](#)

1563 [Yao F, Wang C, Dong D, et al. High-resolution map of urban surface water using ZY-3](#)

1564 [multi-spectral imagery\[J\]. Remote Sensing, 2015, 7\(9\): 12336-12355.](#)

1565 [Yao F, Wang J, Yang K, et al. Lake storage variation on the endorheic Tibetan Plateau](#)

1566 [and its attribution to climate change since the new millennium\[J\]. Environmental](#)

1567 [Research Letters, 2018, 13\(6\): 064011.](#)

1568 Zhang B, Li J S, Shen Q, et al. Recent research progress on long time series and large
1569 scale optical remote sensing of inland water [J]. National Remote Sensing Bulletin,
1570 2021, 25(1): 37-52

1571 Zhang G Q, Yao T D, Chen W F, et al. Regional differences of lake evolution across
1572 China during 1960s—2015 and its natural and anthropogenic causes [J]. Remote
1573 Sensing of Environment, 2019, 221: 386-404

1574 Zhang Y L. Progress and prospect in lake optics: a review [J]. Journal of Lake Sciences,
1575 2011, 23(4): 483-497

1576 Zhao G, Gao H. Automatic correction of contaminated images for assessment of
1577 reservoir surface area dynamics[J]. Geophysical Research Letters, 2018, 45(12):
1578 6092-6099.

1579 Zhou W, Wang L, Li D, et al. Spatial pattern of lake evaporation increases under global
1580 warming linked to regional hydroclimate change [J]. Communications Earth &
1581 Environment, 2021, 2(1): 255.

1582 ~~Adrian R, O'Reilly C M, Zagarese H, et al. Lakes as sentinels of climate change [J].~~
1583 ~~Limnology and Oceanography, 2009, 54(6part2): 2283-2297~~

1584 ~~Bergé-Nguyen M, Crétaux J F. Inundations in the Inner Niger Delta: Monitoring and~~
1585 ~~analysis using MODIS and global precipitation datasets [J]. Remote Sensing, 2015,~~
1586 ~~7(2): 2127-2151.~~

1587 ~~Busker T, de Roo A, Gelati E, et al. A global lake and reservoir volume analysis using~~
1588 ~~a surface water dataset and satellite altimetry[J]. Hydrology and Earth System~~
1589 ~~Sciences, 2019, 23(2): 669-690.—~~

1590 Cao Z G, Ma R H, Duan H T, et al. A machine learning approach to estimate
1591 chlorophyll-a from Landsat 8 measurements in inland lakes [J]. *Remote Sensing*
1592 *of Environment*, 2020, 248: 111974

1593 Cao Z G, Ma R H, Duan H T, et al.. Effects of broad bandwidth on the remote sensing
1594 of inland waters: implications for high spatial resolution satellite data applications
1595 [J]. *ISPRS Journal of Photogrammetry and Remote Sensing*, 2019, 153: 110-122

1596 Carroll M L, Townshend J R G, DiMiceli C M, et al. Shrinking lakes of the Arctic:
1597 Spatial relationships and trajectory of change[J]. *Geophysical Research Letters*,
1598 2011, 38(20).

1599 Cooley S W, Smith L C, Stepan L, et al. Tracking dynamic northern surface water
1600 changes with high-frequency planet CubeSat imagery[J]. *Remote Sensing*, 2017,
1601 9(12): 1306.

1602 Donchyts G, Baart F, Winsemius H, et al. Earth's surface water change over the past 30
1603 years[J]. *Nature Climate Change*, 2016, 6(9): 810-813.

1604 Grant L, Vanderkelen I, Gudmundsson L, et al. Attribution of global lake systems change
1605 to anthropogenic forcing[J]. *Nature Geoscience*, 2021, 14(11):849-854.

1606 Huang C, Chen Y, Zhang S, et al. Detecting, extracting, and monitoring surface water
1607 from space using optical sensors: A review[J]. *Reviews of Geophysics*, 2018, 56(2):
1608 333-360.

1609 Jeppesen E, Meerhoff M, Davidson T, et al. Climate change impacts on lakes: an
1610 integrated ecological perspective based on a multi-faceted approach, with special
1611 focus on shallow lakes[J]. *Journal of Limnology*, 2014, 73.

1612 ~~Klein I, Gessner U, Dietz A J, et al. Global WaterPack—A 250 m resolution dataset~~
1613 ~~revealing the daily dynamics of global inland water bodies[J]. Remote sensing of~~
1614 ~~environment, 2017, 198: 345-362.~~

1615 ~~Kravitz J, Matthews M, Lain L, et al. Potential for high fidelity global mapping of~~
1616 ~~common inland water quality products at high spatial and temporal resolutions~~
1617 ~~based on a synthetic data and machine learning approach[J]. Frontiers in~~
1618 ~~Environmental Science, 2021, 9: 58766~~

1619 ~~LABA Zhuoma, DEJI Yangzong, LA Ba, et al. Remote sensing analysis on the area~~
1620 ~~variations of Tangra Yutso in Tibetan Plateau over the past 40 years [J]. Lake~~
1621 ~~Science, 2017, 29(02): 480-489.~~

1622 ~~Li, L., Long, D., Wang, Y. et al. Global dominance of seasonality in shaping lake-~~
1623 ~~surface extent dynamics. Nature (2025). [https://doi.org/10.1038/s41586-025-](https://doi.org/10.1038/s41586-025-09046-3)~~
1624 ~~09046-3~~

1625 ~~Li M, Yan D H, Liu S H, et al, Variation Characteristics of Water Surface Area and~~
1626 ~~Water Storage Capacity of Namucuo Lake in Recent 40 Years [J]. Water Resources~~
1627 ~~and Power, 2017, 35 (02): 41-43+52.~~

1628 ~~Liu Y B, Wu G P, Zhao X S, et al. Remote sensing for watershed hydrology: issues and~~
1629 ~~challenges [J]. Advances in Earth Science, 2020, 35(5): 488-496~~

1630 ~~Liu Z W, Su Y L and Yang L. Limnology is a multidisciplinary and integrative science~~
1631 ~~for studying inland waters: with special reference to the challenges and~~
1632 ~~opportunities for the development of limnology in China [J]. Journal of Lake~~
1633 ~~Sciences, 2020, 32(5): 1244-1253~~

1634 ~~Ma R H, Duan H T, Hu C M, et al. half-century of changes in China's lakes: global~~
1635 ~~warming or human influence? [J]. Geophysical Research Letters, 2010, 37(24):~~
1636 ~~L24106~~

1637 ~~Ma R H, Yang G S, Duan H T, et al. China's lakes at present: number, area and spatial~~
1638 ~~distribution [J]. Science China Earth Sciences, 2011, 54(2): 283-289~~

1639 ~~Ma Y, Xu N, Zhang W H, et al. Increasing water levels of global lakes between 2003~~
1640 ~~and 2009 [J]. IEEE Geoscience and Remote Sensing Letters, 2020b, 17(2): 187-~~
1641 ~~191~~

1642 ~~McFeeters S K. The use of the Normalized Difference Water Index (NDWI) in the~~
1643 ~~delineation of open water features[J]. International journal of remote sensing, 1996,~~
1644 ~~17(7): 1425-1432.~~

1645 ~~Mouw C B, Greb S, Aurin D, et al. Aquatic color radiometry remote sensing of coastal~~
1646 ~~and inland waters: challenges and recommendations for future satellite missions~~
1647 ~~[J]. Remote Sensing of Environment, 2015, 160: 15-30~~

1648 ~~Palmer S C J, Kutser T and Hunter P D. Remote sensing of inland waters: challenges,~~
1649 ~~progress and future directions [J]. Remote Sensing of Environment, 2015, 157: 1-~~
1650 ~~8~~

1651 ~~Pekel J F, Cottam A, Gorelick N, et al. High-resolution mapping of global surface water~~
1652 ~~and its long-term changes [J]. Nature, 2016, 540(7633): 418-422~~

1653 ~~Pekel J F, Vancutsem C, Bastin L, et al. A near real-time water surface detection method~~
1654 ~~based on HSV transformation of MODIS multi-spectral time-series data[J].~~
1655 ~~Remote sensing of environment, 2014, 140: 704-716.~~

1656 ~~Pieken A H, Hansen M C, Hancher M, et al. Mapping and sampling to characterize~~
1657 ~~global inland water dynamics from 1999 to 2018 with full Landsat time-series [J].~~
1658 ~~Remote Sensing of Environment, 2020, 243: 111792~~

1659 ~~Plug L J, Walls C, Scott B M. Tundra lake changes from 1978 to 2001 on the~~
1660 ~~Tuktoyaktuk Peninsula, western Canadian Arctic[J]. Geophysical Research~~
1661 ~~Letters, 2008, 35(3).~~

1662 ~~Preston D L, Caine N, McKnight D M, et al. Climate regulates alpine lake ice cover~~
1663 ~~phenology and aquatic ecosystem structure[J]. Geophysical Research Letters,~~
1664 ~~2016, 43(10): 5353-5360.~~

1665 ~~Råman Vinnå L, Medhaug I, Schmid M, et al. The vulnerability of lakes to climate~~
1666 ~~change along an altitudinal gradient[J]. Communications Earth & Environment,~~
1667 ~~2021, 2(1): 35.~~

1668 ~~Rossow W B, Schiffer R A. Advances in understanding clouds from ISCCP[J]. Bulletin~~
1669 ~~of the American Meteorological Society, 1999, 80(11): 2261-2288.—~~

1670 ~~Schmid M, Hunziker S, Wüest A. Lake surface temperatures in a changing climate: a~~
1671 ~~global sensitivity analysis[J]. Climatic change, 2014, 124: 301-315.~~

1672 ~~Secretariat G. Implementation plan for the global observing system for climate in~~
1673 ~~support of the UNFCCC (2010 Update) [C]//Proceedings of the Conference of the~~
1674 ~~Parties (COP), Copenhagen, Denmark. 2009: 7-18.~~

1675 ~~Shen M, Duan H T, Cao Z G, et al. Determination of the downwelling diffuse~~
1676 ~~attenuation coefficient of lake water with the Sentinel 3A OLCI [J]. Remote~~
1677 ~~Sensing, 2017, 9(12): 1246~~

1678 ~~Tao S, Fang J, Zhao X, et al. Rapid loss of lakes on the Mongolian Plateau[J].~~
1679 ~~Proceedings of the National Academy of Sciences, 2015, 112(7): 2281-2286.~~

1680 ~~Tong Y, Feng L, Wang X, et al. Global lakes are warming slower than surface air~~
1681 ~~temperature due to accelerate devaporation [J]. Nature Water, 2023, 1(11): 929-940~~

1682 ~~Vincent W F. Effects of climate change on lakes[J]. 2009.~~

1683 ~~Wang J, Song C, Reager J T, et al. Recent global decline in endorheic basin water~~
1684 ~~storages[J]. Nature geoscience, 2018, 11(12): 926-932.~~

1685 ~~Woolway R I, Kraemer B M, Lenters J D, et al. Global lake responses to climate~~
1686 ~~change[J]. Nature Reviews Earth & Environment, 2020, 1(8): 388-403.~~

1687 ~~Yang G S, Ma R H, Zhang L, et al. Lake status, major problems and protection strategy~~
1688 ~~in China [J]. Journal of Lake Sciences, 2010, 22(6): 799-810~~

1689 ~~Yao F, Wang C, Dong D, et al. High-resolution map of urban surface water using ZY-3~~
1690 ~~multi-spectral imagery[J]. Remote Sensing, 2015, 7(9): 12336-12355.~~

1691 ~~Yao F, Wang J, Yang K, et al. Lake storage variation on the endorheic Tibetan Plateau~~
1692 ~~and its attribution to climate change since the new millennium[J]. Environmental~~
1693 ~~Research Letters, 2018, 13(6): 064011.~~

1694 ~~Zhang B, Li J S, Shen Q, et al. Recent research progress on long time-series and large~~
1695 ~~scale optical remote sensing of inland water [J]. National Remote Sensing Bulletin,~~
1696 ~~2021, 25(1): 37-52~~

1697 ~~Zhang G Q, Yao T D, Chen W F, et al. Regional differences of lake evolution across~~
1698 ~~China during 1960s—2015 and its natural and anthropogenic causes [J]. Remote~~
1699 ~~Sensing of Environment, 2019, 221: 386-404~~

1700 ~~Zhang Y L. Progress and prospect in lake optics: a review [J]. Journal of Lake Sciences,~~
1701 ~~2011, 23(4): 483-497~~

1702 ~~Zhao G, Gao H. Automatic correction of contaminated images for assessment of~~
1703 ~~reservoir surface area dynamics[J]. Geophysical Research Letters, 2018, 45(12):~~
1704 ~~6092-6099.~~

1705 ~~Zhou W, Wang L, Li D, et al. Spatial pattern of lake evaporation increases under global~~
1706 ~~warming linked to regional hydroclimate change [J]. Communications Earth &~~
1707 ~~Environment, 2021, 2(1): 255.~~